Single-Anchor Two-Way Localization Bounds for 5G mmWave Systems

Zohair Abu-Shaban, *Senior Member, IEEE*, Henk Wymeersch, *Senior Member, IEEE*, Thushara Abhayapala, *Senior Member, IEEE*, and Gonzalo Seco-Granados, *Senior Member, IEEE*

***Abstract*—Recently, millimeter-wave (mmWave) 5G localization has been shown to be to provide centimeter-level accuracy, lending itself to many location-aware applications, e.g., connected autonomous vehicles (CAVs). One assumption usually made in the investigation of localization methods is that the user equipment (UE), i.e., a CAV, and the base station (BS) are time synchronized. In this paper, we remove this assumption and investigate two two-way localization protocols: (i) a round-trip localization protocol (RLP), whereby the BS and UE exchange signals in two rounds of transmission and then localization is achieved using the signal received in the second round; (ii) a collaborative localization protocol (CLP), whereby localization is achieved using the signals received in the two rounds. We derive the position and orientation error bounds applying beamforming at both ends and compare them to the traditional one-way localization. Our results show that mmWave localization is mainly limited by the angular rather than the temporal estimation and that CLP significantly outperforms RLP. Our simulations also show that it is more beneficial to have more antennas at the BS than at the UE.**

***Index Terms*—5G, beamforming, collaborative communications, Fisher information, localization, orientation error bound, position error bound, positioning.**

I. Introduction

THE FIFTH generation of mobile communication (5G) using millimeter-wave technology (mmWave) will be the first generation to integrate the location information in the network design and optimization [1], [2], for example through, beamforming [3], pilot assignment [4], and resource allocation [5].

Localization error in mmWave 5G has been shown to be in the order of centimeters, making location-aware applications in 5G much more attractive than ever before. Such applications including targeted content delivery [6], vehicular communication [7], and assisted living systems [8]. Of particular interest are systems of connected autonomous vehicles (CAVs) [9], which are a typical use case of 5G communication [10], and air-ground communication with unmanned aerial vehicles (UAVs) [11].

Due to the deployment of arrays with a high number of antennas at the transmitter and the receiver, and the utilization of large bandwidth [12]–[16], localization with a single base station (BS) can be seen as the ultimate localization strategy for 5G. With the high number of antennas, the directions of arrival (DOA) and departure (DOD) can be estimated with a very low error [17], while the large bandwidth enables a highly accurate estimation of the time of arrival (TOA) [18]–[21], i.e., a low-error range estimate. Subsequently, combining the spatial and temporal estimates, the user equipment (UE) location[1] can be estimated. On the other hand, some papers consider mmWave channels estimation in the beamspace [22]–[24], so in principle, the AOA and AOD can be deduced directly from the channel estimate. However, the estimation in the beamspace does not show how to estimate the TOA.

Recently, the accuracy of single-anchor[2] localization for 5G mmWave systems has been studied in several papers in terms of position (PEB) and orientation error bounds (OEB). PEB and OEB are theoretical bounds that are used to benchmark location estimation techniques, and hence they are measures of the optimality of such techniques. In [25], the UE PEB and OEB of 2D localization were investigated using uniform linear arrays in 5G mmWave systems. Moreover, [26] and [27] derived, with different approaches, the PEB and OEB for mmWave 3D localization using arrays with arbitrary geometry. The results in [25]–[27] showed a 5G mmWave localization performance with an error in the order of centimeters. However, one important, yet usually overlooked, requirement for localization is the synchronization of BS and UE. For example, [25] and [27] assume that the BS

Manuscript received August 4, 2019; revised December 4, 2019 and March 4, 2020; accepted April 6, 2020. Date of publication April 13, 2020; date of current version June 18, 2020. This work was supported in part by the Australian Government's Research Training Program (RTP), in part by the Horizon 2020 projects HIGHTS (High precision positioning for cooperative ITS applications) MG-3.5a-2014-636537 and 5GCAR (Fifth Generation Communication Automotive Research and innovation), in part by the VINNOVA COPPLAR, in part by the Strategic Vehicle Research and Innovation under Grant 2015-04849, and in part by the Spanish Ministry of Science and Innovations under Grants TEC2017-89925-R and TEC2017-90808-REDT, and by the ICREA Academia Program. A part of this article was presented at the IEEE GLOBECOM Workshops, Abu Dhabi, UAE, Dec. 2018. The review of this article was coordinated by Prof. H. Zhu. *(Corresponding author: Zohair Abu-Shaban.)*

Zohair Abu-Shaban is with the School of Engineering and Information Technology, University of New South Wales, Canberra, NSW 2618, Australia (e-mail: zohair.abushaban@ieee.org).

Henk Wymeersch is with the Department of Signals and Systems, Chalmers University of Technology 412 96, Göteborg, Sweden (e-mail: henkw@chalmers.se).

Thushara Abhayapala is with the Research School of Engineering (RSEng), Australian National University, Canberra 0200, Australia (e-mail: thushara.abhayapala@anu.edu.au).

Gonzalo Seco-Granados is with the Department of Telecommunications and Systems Engineering, Universitat Autònoma de Barcelona 08193, Bellaterra, Barcelona, Spain (e-mail: gonzalo.seco@uab.cat).

Digital Object Identifier 10.1109/TVT.2020.2987039

[1] In this article, we use the terms *location/localization* and *position/positioning* interchangeably.

[2] In mobile networks, anchor refers to the BS, whose position and orientation are known.

and UE are perfectly synchronized, while [26] assumes coarse synchronization, and includes a residual synchronization error in their localization model. Synchronization can be avoided by the use of two-way ranging methods [28]–[30], where the time-of-flight is utilized to estimate the range and clock bias, or three-way ranging [28] and multi-way ranging [31], [32] to additionally estimate higher-order artifacts such as clock drift and skew. However, such methods have not been evaluated for mmWave systems. Such systems possess different features, including highly sparse channels and directional transmission, making the estimation of the angles of arrival and departure as relevant to localization as the time of arrival. Our work is the first to consider such a scenario and investigate the associated two-way positioning performance that is a function of the spatio-temporal properties of the channel.

In this paper, we propose two-way localization (TWL), whereby a known signal is transmitted from the first device, the BS or the UE, to the second device that, in turn, responds by sending another known signal, after which the relative location and orientation of the devices can be estimated. We study the PEB and OEB under line-of-sight (LOS) communication for two protocols: (i) *Round-trip Localization Protocol (RLP),* where the second device waits for a pre-agreed interval, from the time the first signal is received, before sending another signal to the first device, upon which localization is based; and (ii) *Collaborative Localization Protocol (CLP),* where the second device sends back the received signal to the first device, and localization is based on both signals. By their nature, these bounds are theoretical and serve as a means to determine performance benchmarks to assess location estimation techniques, to design localization systems, and to determine when the location and orientation can be potentially estimated. Our main contributions are:

- Introducing RLP and CLP for LOS 5G mmWave signals and their analysis in terms of the localization bounds.
- For the two protocols, we derive the Fisher information matrices (FIMs) of the position and orientation, and consequently the PEB and OEB, with the timing bias between the BS and UE as a nuisance parameter.
- We investigate the impact of the number of antennas at BS and UE, as well as the bandwidth, and show that, in contrast to the standard two-way ranging methods [28]–[30], the TWL performance in mmWave multiple-input multiple-output (MIMO) systems depends on the device that initiates the protocol.

The initial results of the RLP were presented briefly in [33], while in this paper, while in this paper, we i) discuss RLP in more detail, ii) provide CLP as additional protocol, and iii) present more in-depth performance analysis and insightful results on both protocols.

The rest of the paper is organized as follows. The system model, including the considered geometry, channel model and beamforming, is described in Section II, while the proposed protocols are outlined in Section III. Subsequently, FIM basics are introduced at the outset of Section IV, before proceeding to derive the PEB and OEB for both protocols. The numerical simulation results are given in Section V, while the conclusions are highlighted in Section VI.

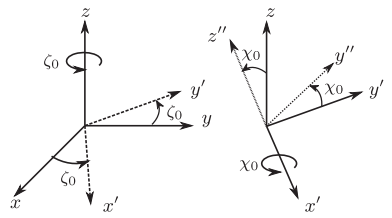

Fig. 1. Two-step rotation: The first rotation is around the z-axis, creating x' and y' axes. The second rotation is around x', creating y'' and z'' axes.

II. System Model

A. System Geometry

Consider a BS located at the origin of the 3D space with zero-orientation angles, and a UE located at a fixed unknown position $\mathbf{p} \triangleq [p_x, p_y, p_z]^{\mathrm{T}}$ with unknown orientation angles $\mathbf{o} \triangleq [\zeta_0, \chi_0]^{\mathrm{T}}$. As illustrated in Fig. 1, we define ζ_0 as the rotation angle around the $z-$axis, which yields new coordinate axes x', y' and z. Similarly, χ_0 is defined as the rotation angle around the $x'-$axis. Both BS and UE are equipped with antenna arrays of arbitrary but known geometries and communicate through a mmWave channel.

Although a device may have up to three rotation angles, we consider two angles because the estimation of three orientation angles is not possible with only LOS communication. Hence, our formulation is representative of practical applications characterized by two rotation angles,[3] such as near-static[4]

Our objective is to derive the performance bounds of estimating $\mathbf{p}$ and $\mathbf{o}$ via TOA, DOA, and DOD estimation, in the presence of the unknown nuisance parameters, i.e., the timing offset between the BS and UE clocks, B, and the unknown channel. This is done for the RLP and CLP protocols described in Section III. Our analysis considers the effect of all these unknown parameters. If a subset of the parameters is known, the bounds become lower and can be easily derived as special cases.

B. Channel Model

We consider protocols initiated by either the BS or UE. The device initiating the protocol is denoted by D_1, and the responding device by D_2. In the presence of multipath, mmWave paths are orthogonal and information-additive [8], [34], [35], and hence do not interfere with one another. Moreover, the LOS path is stronger than the NLOS paths and hence provides the highest useful information in terms of positioning, while also being easy to isolate based on the signal power profile. Therefore, although we assume that the exchange of signals occurs via the LOS

[3]This corresponds for instance to a vehicle that can turn left and right (ζ_0) or ascend and descend (χ_0), but not slip or flip.

[4]We study positioning with a short signal snapshot, during which the UE moves by a negligible distance. Subsequently, there has to be another layer where the snapshot positions are filtered through tracking techniques and mobility models, but this is out of the scope of this paper.

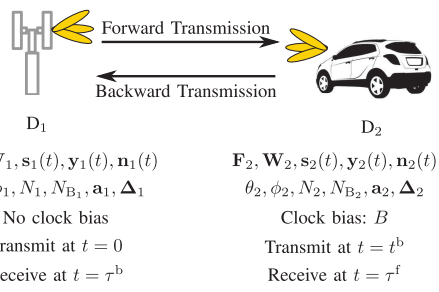

Fig. 2. Summary of parameters at D_1 and D_2. Although D_1 and D_2 in the figure are BS and UE, this can be reversed.

path, our analysis is valid even when there are NLOS paths. In any case, the presence of NLOS paths would assist localization, unlike in other systems, e.g., GPS, where multipath can limit the performance [8], [34], [35].

Remark 1 (Notation): All parameters related to D_1 and D_2 are denoted by the subscripts "1" and "2," respectively. Moreover, the superscripts "f" and "b" are used to relate the parameters to the forward and backward transmissions, respectively. Also, unless otherwise stated, all the provided times are with respect to the clock of D_1, which is considered a global clock. See Fig. 2.

Let $h^{\mathrm{f}} \triangleq \beta^{\mathrm{f}} \exp(j\psi^{\mathrm{f}})$ be the complex LOS path gain in the forward direction, N_1 and N_2 be the number of antennas at D_1 and D_2, respectively, and (θ_1, ϕ_1) and (θ_2, ϕ_2) be the forward DOD and DOA at D_1 and D_2, respectively. Also, define $\boldsymbol{\vartheta} \triangleq [\theta_1, \phi_1, \theta_2, \phi_2]^{\mathrm{T}}$.

The *forward* signal, from D_1 to D_2, undergoes a forward channel given by [15]

$$\mathbf{H}^{\mathrm{f}}(\boldsymbol{\vartheta}, \tau^{\mathrm{f}}, h^{\mathrm{f}}) \triangleq \mathbf{H}^{\mathrm{f}}_{\mathrm{s}}(\boldsymbol{\vartheta}, h^{\mathrm{f}})\delta(t - \tau^{\mathrm{f}}), \in \mathbb{C}^{N_2 \times N_1} \quad (1)$$

where $\delta(t)$ is the Dirac delta function, $t = \tau^{\mathrm{f}}$ is the perceived TOA at D_2, and

$$\mathbf{H}^{\mathrm{f}}_{\mathrm{s}}(\boldsymbol{\vartheta}, h^{\mathrm{f}}) \triangleq \sqrt{N_1 N_2} h^{\mathrm{f}} \mathbf{a}_2(\theta_2, \phi_2)\mathbf{a}_1^{\mathrm{T}}(\theta_1, \phi_1). \quad (2)$$

$\mathbf{a}_i, i \in \{1, 2\}$ is the response vectors at D_i given by

$$\mathbf{a}_i(\theta_i, \phi_i) \triangleq \frac{1}{\sqrt{N_i}} e^{-j\boldsymbol{\Delta}_i^{\mathrm{T}}\mathbf{k}(\theta_i, \phi_i)}, \quad \in \mathbb{C}^{N_i} \quad (3)$$

where $\mathbf{k}(\theta, \phi) = \frac{2\pi}{\lambda}[\cos\phi \sin\theta, \sin\phi \sin\theta, \cos\theta]^{\mathrm{T}}$ is the wavenumber vector, λ is the wavelength, $\boldsymbol{\Delta}_i \in \mathbb{C}^{3 \times N_i}$ is a matrix whose columns contain the 3D Cartesian coordinates of the array elements of D_i in meters. For brevity, we drop the angle parameters from the notation of $\mathbf{a}_i$.

Similarly, the backward channel from D_2 to D_1 is defined as

$$\mathbf{H}^{\mathrm{b}}(\boldsymbol{\vartheta}, \tau^{\mathrm{b}}, h^{\mathrm{b}}) \triangleq \mathbf{H}^{\mathrm{b}}_{\mathrm{s}}(\boldsymbol{\vartheta}, h^{\mathrm{b}})\delta(t - \tau^{\mathrm{b}}) \in \mathbb{C}^{N_1 \times N_2}, \quad (4)$$

where $h^{\mathrm{b}} \triangleq \beta^{\mathrm{b}} \exp(j\psi^{\mathrm{b}})$ and

$$\mathbf{H}^{\mathrm{b}}_{\mathrm{s}}(\boldsymbol{\vartheta}, h^{\mathrm{b}}) \triangleq \sqrt{N_1 N_2} h^{\mathrm{b}} \mathbf{a}_1(\theta_1, \phi_1)\mathbf{a}_2^{\mathrm{T}}(\theta_2, \phi_2), \quad (5)$$

where τ^{b} denotes the local TOA at D_1.

Note that (1)–(5) represent an accepted model for mmWave channels [15]. Unlike cmWave channels, which experience rich scattering and relatively low propagation losses, mmWave channels are sparse and have high propagation losses, leading to weaker NLOS paths than LOS. Furthermore, due to the large temporal and spatial resolution of mmWave massive MIMO systems, reflections can be resolved if there are NLOS paths, and the parameters of the LOS can be estimated without noticeable impact from the NLOS [27]. Thus, for the sake of analysis, one can consider that the LOS-only situation is representative of scenarios where the reflections are resolvable, if present at all. For the cases where the LOS path is blocked, it has been shown recently that the probability of localization via NLOS paths alone is only about 12% [36].

C. Precoding and Combining

The signal transmitted from D_1 is modeled by $\sqrt{E_{\mathrm{t}}}\mathbf{F}_1\mathbf{s}_1(t)$, where E_{t} is the transmitted energy per symbol, and $\mathbf{F}_1 \in \mathbb{C}^{N_1 \times N_{\mathrm{B},1}}$ is the transmit beamforming matrix at D_1 containing $N_{\mathrm{B},1}$ analog beamforming vectors. The pilot signal $\mathbf{s}_1(t) \triangleq [s_{1,1}(t), s_{1,2}(t), \ldots, s_{1,N_{\mathrm{B}_1}}(t)]^{\mathrm{T}}$ is written as

$$s_{1,b}(t) = \sum_{\ell=0}^{N_{\mathrm{s}}-1} a_{1,\ell}^{(b)} g(t - \ell T_{\mathrm{s}}), \; 1 \le b \le N_{\mathrm{B}_1}, \quad (6)$$

where $a_{1,\ell}^{(b)}$ are known unit-energy pilot symbols transmitted over the b^{th} beam from D_1, and $g(t)$ is a unit-energy pulse with a symmetric power spectral density (PSD), denoted by $|G(f)|^2$. In (6), N_{s} is the number of pilot symbols and T_{s} is the symbol duration, leading to a total observation time of $T_{\mathrm{o}} \approx N_{\mathrm{s}}T_{\mathrm{s}}$. Note that we keep the transmitted power fixed with N_1 by setting $\mathrm{Tr}(\mathbf{F}_1^{\mathrm{H}}\mathbf{F}_1) = 1$, and $\mathbf{s}_1(t)\mathbf{s}_1^{\mathrm{H}}(t) = \mathbf{I}_{N_{\mathrm{B}_1}}$, where $\mathrm{Tr}(\cdot)$ denotes the matrix trace, and $\mathbf{I}_{N_{\mathrm{B}_1}}$ is the N_{B_1}-dimensional identity matrix. Similarly, $\mathbf{W}_2 \in \mathbb{C}^{N_2 \times N_{\mathrm{B},2}}$ denotes the receive beamforming matrix at D_2 containing $N_{\mathrm{B},2}$ analog beamforming vectors.

In backward transmission, D_2 transmits $\mathbf{s}_2(t)$ via a beamforming matrix, $\mathbf{F}_2$ containing N_{B_2} beams, while D_1 receives via a beamforming matrix, $\mathbf{W}_1$ containing N_{B_1} beams. Both $\mathbf{F}_2$ and $\mathbf{W}_1$ are defined similar to $\mathbf{W}_2$ and $\mathbf{F}_1$, respectively, but with possibly different beam directions.

III. Synchronization and Localization Protocols

In this section, we discuss how clock synchronization can be addressed in 5G mmWave. We start by presenting a general formulation of two-way localization, which we then specify for two different protocols with the aid of Fig. 3.

A. General Operation

We take the clock at D_1 as a reference and assume that D_2 has a *clock bias*,[5] B, with respect to it. We also denote the nominal TOA by $\tau = \|\mathbf{p}\|/c$, where c is the speed of light.

During the **forward transmission**, the signal received after beamforming at D_2 is given by

$$\mathbf{y}_2(t) = \sqrt{E_{\mathrm{t}}}\mathbf{W}_2^{\mathrm{H}}\mathbf{H}^{\mathrm{f}}_{\mathrm{s}}(h^{\mathrm{f}}, \boldsymbol{\vartheta})\mathbf{F}_1\mathbf{s}_1(t - \tau^{\mathrm{f}}) + \mathbf{n}_2(t), \quad (7)$$

[5]Bias is modeled as an unknown constant, as we consider a snapshot observation over which it is assumed to remain unchanged.

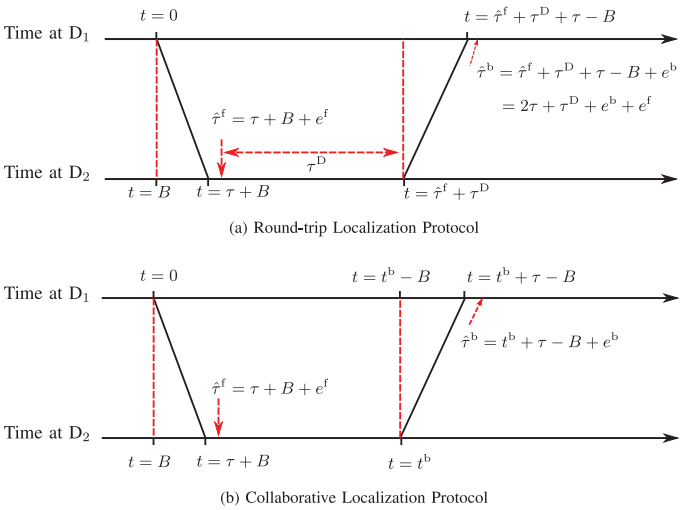

Fig. 3. The timeline of the studied TWL protocols.

where $\mathbf{n}_2(t)$ is zero-mean additive *spatially-correlated* Gaussian noise, since the received signals are observed at the beamformer output. Therefore, the corresponding noise auto-covariance matrix is $\mathbf{R}_{\mathrm{n}2} = N_0 \mathbf{W}_2^{\mathrm{H}} \mathbf{W}_2$, where N_0 is the noise PSD. We assume that N_0 is identical at BS and UE. Moreover, the delay at D_2 is

$$\tau^{\mathrm{f}} = \tau + B. \tag{8}$$

Similarly, in the **backward transmission**, the signal received after beamforming at D_1 is

$$\mathbf{y}_1(t) = \sqrt{E_{\mathrm{t}}} \mathbf{W}_1^{\mathrm{H}} \mathbf{H}_{\mathrm{s}}^{\mathrm{b}}(\boldsymbol{\vartheta}, h^{\mathrm{b}}) \mathbf{F}_2 \mathbf{s}_2(t - \tau^{\mathrm{b}}) + \mathbf{n}_1(t), \tag{9}$$

where $\mathbf{n}_1(t)$ has an auto-covariance matrix $\mathbf{R}_{\mathrm{n}1} = N_0 \mathbf{W}_1^{\mathrm{H}} \mathbf{W}_1$. Note that the backward transmission is initiated by D_2 at a time $t = t^{\mathrm{b}}$, and that the clock bias of D_2 observed at D_1 is $-B$. Hence, the delay at D_1 is

$$\tau^{\mathrm{b}} = t^{\mathrm{b}} + \tau - B. \tag{10}$$

There are different ways by which the synchronization of the response message from D_2 can be coordinated. In the following, we specify our formulation for two localization protocols, round-trip (RLP) and collaborative (CLP). While τ^{f} is the same for CLP and RLP, their essential difference is in how each one defines t^{b}, the instant at which D_2 sends the reply message (backward). For RLP, D_2 starts transmission after a pre-defined time-interval τ_{D}, taken with reference to its local clock, while in CLP, it starts transmission after t^{b}, taken with reference to the clock of D_2.

B. Round-Trip Localization Protocol (RLP)

Under RLP, D_2 estimates τ^{f} and waits for a pre-agreed delay τ^{D} before transmitting back the signal $\mathbf{s}_2(t)$. In other words,

$$t^{\mathrm{b}} = \hat{\tau}^{\mathrm{f}} + \tau^{\mathrm{D}}, \tag{11}$$

where $(\hat{\cdot})$ denotes the estimated value of a parameter. See Fig. 3(a). We now introduce $e^{\mathrm{f}} \triangleq \hat{\tau}^{\mathrm{f}} - \tau^{\mathrm{f}}$ (and similarly $e^{\mathrm{b}} \triangleq \hat{\tau}^{\mathrm{b}} - \tau^{\mathrm{b}}$). Substituting (11) in (10), then using (8), it can be shown that D_1 receives the signal $\mathbf{y}_1(t)$ at time

$$\tau^{\mathrm{b}} = \hat{\tau}^{\mathrm{f}} + \tau^{\mathrm{D}} + \tau - B = 2\tau + e^{\mathrm{f}} + \tau^{\mathrm{D}}, \tag{12}$$

Finally, based on $\mathbf{y}_1(t)$, D_1 estimates $\hat{\tau}^{\mathrm{b}}$ and eventually determines $\mathbf{p}$, and $\mathbf{o}$. Note that B in the forward and backward transmissions cancel out and need not be estimated at D_2.

C. Collaborative Localization Protocol (CLP)

Unlike RLP, under CLP D_2 sends back a signal $\mathbf{s}_2(t)$ at a pre-agreed time instant $t = t^{\mathbf{b}}$. The value of $t = t^{\mathbf{b}}$ can be chosen to be large enough to avoid overlapping with the preceding transmission of $\mathbf{s}_1(t)$. Given that D_2 decides that the instant $t = t^{\mathbf{b}}$ has occurred based on its own clock, then the TOA measured by D_1 in its own time scale is given by (10).

In parallel, D_1 also receives $\mathbf{y}_2(t)$ via an error-free feedback[6] link that can possibly be established using a microwave channel. Finally, based on $\mathbf{y}_1(t)$ *and* $\mathbf{y}_2(t)$, D_1 estimates $\mathbf{p}$ and $\mathbf{o}$. Comparing (12) and (10), it can be seen that B needs to be estimated under CLP, unlike RLP.

IV. Derivation of the Two-Way Position and Orientation Error Bounds

After defining the system model and the communication protocols that govern the observations collection, we now proceed to define and derive PEB and OEB as performance metrics for the two protocols. These metrics are lower bounds on the performance of any estimator and can thus be used to benchmark localization algorithms. In fact, these bounds are tight for the problem under investigation. That is, the performance of well-designed practical algorithms approaches these bounds in the localization scenarios of interest [25]. Therefore, analyzing the protocols in terms of the PEB and the OEB has the advantage of being representative of practical designs without the need for proposing detailed estimation algorithms. Moreover, since the PEB and OEB can often be computed in closed forms, another advantage is that they provide fundamental insights into the localization problem.

The PEB and OEB are derived from the FIM, a notion we discuss first in Section IV-A. Then, we apply the FIM to the estimation of channel parameters in the forward and backward transmissions in Section IV-B. This allows us to compute the PEB and OEB of RLP and CLP in Sections IV-C and IV-D, respectively, and make a quantitative performance comparison in Section IV-E.

A. Basic FIM Concepts

In this section, we digress to provide a brief introduction to the notion of FIM and Equivalent FIM (EFIM), useful in the analysis of the TWL protocols. For more background on Fisher information, the reader is referred to [37].

[6]To give a general exposition, we assume that the second signal is sent back entirely. However, there are some alternatives that facilitate obtaining the same bounds in a more practical way, like feeding back the parameters estimated from $\mathbf{y}_2(t)$ instead of the actual $\mathbf{y}_2(t)$. Any errors introduced in the transmission are assumed to be corrected via layers of coding and ARQ.

Given a vector observation $\mathbf{y}$ and an unknown deterministic vector parameter $\boldsymbol{\theta}$, related by $\mathbf{y} = \mathbf{h}(\boldsymbol{\theta}) + \mathbf{n}$, where $\mathbf{n} \sim \mathcal{N}(\mathbf{0}, \boldsymbol{\Sigma})$, with $\boldsymbol{\Sigma}$ independent of $\boldsymbol{\theta}$, then the FIM $\mathbf{J}_{\boldsymbol{\theta}}$ is a positive semi-definite matrix, defined as $\mathbf{J}_{\boldsymbol{\theta}} = \nabla_{\boldsymbol{\theta}}\mathbf{h}^{\mathrm{T}}(\boldsymbol{\theta})\boldsymbol{\Sigma}^{-1}(\nabla_{\boldsymbol{\theta}}\mathbf{h}(\boldsymbol{\theta}))$. Under certain regularity conditions, the inverse of the FIM (provided it exists) serves as a lower bound on the estimation error covariance of any unbiased estimator:

$$\mathbb{E}\{(\hat{\boldsymbol{\theta}} - \boldsymbol{\theta})(\hat{\boldsymbol{\theta}} - \boldsymbol{\theta})^{\mathrm{T}}\} \succeq \mathbf{J}_{\boldsymbol{\theta}}^{-1}, \tag{13}$$

where the expectation is over the noise and $\mathbf{A} \succeq \mathbf{B}$ means that $\mathbf{A} - \mathbf{B}$ is a positive semidefinite matrix. The Cramér-Rao lower bound (CRLB) is computed as the diagonal of the inverse FIM.

If instead of $\boldsymbol{\theta}$ we need the FIM of $\boldsymbol{\phi} = f(\boldsymbol{\theta})$, we can apply a transformation on the FIM.

Definition 1 (FIM Transformation): Given the FIM $\mathbf{J}_{\boldsymbol{\theta}}$ and an injective mapping $\boldsymbol{\theta} = f(\boldsymbol{\phi})$, the FIM $\mathbf{J}_{\boldsymbol{\phi}}$ is given by [37]

$$\mathbf{J}_{\boldsymbol{\phi}} = \boldsymbol{\Upsilon}\mathbf{J}_{\boldsymbol{\theta}}\boldsymbol{\Upsilon}^{\mathrm{T}}, \tag{14}$$

where $\boldsymbol{\Upsilon}$ is a Jacobian matrix with $[\boldsymbol{\Upsilon}]_{i,j} = \partial\boldsymbol{\theta}_i/\partial\boldsymbol{\phi}_j = \partial[f(\boldsymbol{\phi})]_i/\partial\boldsymbol{\phi}_j$.

The EFIM is derived from the FIM, when we are interested only in part of the vector $\boldsymbol{\theta}$.

Definition 2 (Equivalent FIM): Given a parameter vector $\boldsymbol{\theta} \triangleq [\boldsymbol{\theta}_1^{\mathrm{T}}, \boldsymbol{\theta}_2^{\mathrm{T}}]^{\mathrm{T}}$ with associated FIM

$$\mathbf{J}_{\boldsymbol{\theta}} = \begin{bmatrix} \mathbf{J}_{\boldsymbol{\theta}_1} & \mathbf{J}_{\boldsymbol{\theta}_1\boldsymbol{\theta}_2} \\ \mathbf{J}_{\boldsymbol{\theta}_1\boldsymbol{\theta}_2}^{\mathrm{T}} & \mathbf{J}_{\boldsymbol{\theta}_2} \end{bmatrix}, \tag{15}$$

Then, the EFIM of $\boldsymbol{\theta}_1$ is given by Schur complement as [20]

$$\mathbf{J}_{\boldsymbol{\theta}_1}^{\mathrm{e}} = \mathbf{J}_{\boldsymbol{\theta}_1} - \mathbf{J}_{\boldsymbol{\theta}_1\boldsymbol{\theta}_2}\mathbf{J}_{\boldsymbol{\theta}_2}^{-1}\mathbf{J}_{\boldsymbol{\theta}_1\boldsymbol{\theta}_2}^{\mathrm{T}}. \tag{16}$$

Note that according to this definition, $\mathbf{J}_{\boldsymbol{\theta}_1}$ is the FIM of $\boldsymbol{\theta}_1$ if $\boldsymbol{\theta}_2$ were known, and $\mathbf{J}_{\boldsymbol{\theta}_1\boldsymbol{\theta}_2}\mathbf{J}_{\boldsymbol{\theta}_2}^{-1}\mathbf{J}_{\boldsymbol{\theta}_1\boldsymbol{\theta}_2}^{\mathrm{T}}$ is the loss of information due to the uncertainty of $\boldsymbol{\theta}_2$.

Definition 3 (PEB and OEB): Given the equivalent Fisher information matrix of the orientation and the position, $\mathbf{J}_{\mathbf{o},\mathbf{p}}^{\mathrm{e}} \triangleq \mathbf{C}^{-1} \in \mathbb{R}^{5\times5}$, then, the OEB and PEB are defined as [20]

$$\mathrm{OEB} \triangleq \sqrt{[\mathbf{C}]_{1,1} + [\mathbf{C}]_{2,2}}, \tag{17a}$$

$$\mathrm{PEB} \triangleq \sqrt{[\mathbf{C}]_{3,3} + [\mathbf{C}]_{4,4} + [\mathbf{C}]_{5,5}} \tag{17b}$$

B. General FIM for Channel Parameters

For either the forward or the backward transmission, we can compute the FIM of the channel parameters. Focusing on the backward transmission, the FIM of the channel parameters $\boldsymbol{\varphi}^{\mathrm{b}} \triangleq [\boldsymbol{\vartheta}^{\mathrm{T}}, \psi^{\mathrm{b}}, \beta^{\mathrm{b}}, \tau^{\mathrm{b}}]^{\mathrm{T}}$ from the observation $\mathbf{y}_1(t)$ is derived in Appendix A and is shown to be

$$\mathbf{J}_{\boldsymbol{\varphi}^{\mathrm{b}}} \triangleq \begin{bmatrix} \mathbf{J}_{\mathrm{SS}}^{\mathrm{b}} & \mathbf{0}_{5\times2} \\ \mathbf{0}_{2\times5} & \begin{bmatrix} J_{\beta^{\mathrm{b}}}^{\mathrm{b}} & 0 \\ 0 & J_{\tau}^{\mathrm{b}} \end{bmatrix} \end{bmatrix}, \tag{18}$$

where,

$$\mathbf{J}_{\mathrm{SS}}^{\mathrm{b}} = \begin{bmatrix} \mathbf{J}_{\boldsymbol{\vartheta}}^{\mathrm{b}} & \mathbf{J}_{\boldsymbol{\vartheta}\beta^{\mathrm{b}}}^{\mathrm{b}} \\ \left(\mathbf{J}_{\boldsymbol{\vartheta}\beta^{\mathrm{b}}}^{\mathrm{b}}\right)^{\mathrm{T}} & J_{\beta^{\mathrm{b}}}^{\mathrm{b}} \end{bmatrix}, \tag{19}$$

is the FIM corresponding to the spatial parameters of $\mathbf{J}_{\boldsymbol{\varphi}^{\mathrm{b}}}$, such that

$$\mathbf{J}_{\boldsymbol{\vartheta}}^{\mathrm{b}} \triangleq \begin{bmatrix} J_{\theta_1}^{\mathrm{b}} & J_{\theta_1\phi_1}^{\mathrm{b}} & J_{\theta_1\theta_2}^{\mathrm{b}} & J_{\theta_1\phi_2}^{\mathrm{b}} \\ J_{\theta_1\phi_1}^{\mathrm{b}} & J_{\phi_1}^{\mathrm{b}} & J_{\phi_1\theta_2}^{\mathrm{b}} & J_{\phi_1\phi_2}^{\mathrm{b}} \\ J_{\theta_1\theta_2}^{\mathrm{b}} & J_{\phi_1\theta_2}^{\mathrm{b}} & J_{\theta_2}^{\mathrm{b}} & J_{\theta_2\phi_2}^{\mathrm{b}} \\ J_{\theta_1\phi_2}^{\mathrm{b}} & J_{\phi_1\phi_2}^{\mathrm{b}} & J_{\theta_2\phi_2}^{\mathrm{b}} & J_{\phi_2}^{\mathrm{b}} \end{bmatrix}, \tag{20}$$

$$\left(\mathbf{J}_{\boldsymbol{\vartheta}\beta^{\mathrm{b}}}^{\mathrm{b}}\right)^{\mathrm{T}} \triangleq \begin{bmatrix} J_{\theta_1\beta^{\mathrm{b}}}^{\mathrm{b}} & J_{\phi_1\beta^{\mathrm{b}}}^{\mathrm{b}} & J_{\theta_2\beta^{\mathrm{b}}}^{\mathrm{b}} & J_{\phi_2\beta^{\mathrm{b}}}^{\mathrm{b}} \end{bmatrix}. \tag{21}$$

The FIM of $\boldsymbol{\varphi}^{\mathrm{f}} \triangleq [\boldsymbol{\vartheta}^{\mathrm{T}}, \psi^{\mathrm{f}}, \beta^{\mathrm{f}}, \tau^{\mathrm{f}}]^{\mathrm{T}}$ is obtained from the observation $\mathbf{y}_2(t)$ in the same way and exhibits the same structure, as highlighted at the end of Appendix B.

Remark 2: Due to the structure of (18), the delay is always independent of the other channel parameters and can thus be treated separately. It will be convenient to introduce the EFIM of the delay in forward and backward transmissions: we denote by $J_{\tau^{\mathrm{f}}}$ the EFIM of τ^{f}, obtained from applying Definition 2 to the FIM of $[\boldsymbol{\vartheta}^{\mathrm{T}}, \psi^{\mathrm{f}}, \beta^{\mathrm{f}}, \tau^{\mathrm{f}}]^{\mathrm{T}}$ based on the measurement $\mathbf{y}_2(t)$. Similarly, we denote by $J_{\tau^{\mathrm{b}}}$ the EFIM of τ^{b}, obtained from applying Definition 2 to the FIM of $[\boldsymbol{\vartheta}^{\mathrm{T}}, \psi^{\mathrm{b}}, \beta^{\mathrm{b}}, \tau^{\mathrm{b}}]^{\mathrm{T}}$ based on the measurement $\mathbf{y}_1(t)$. Note that, by definition,

$$\mathbb{E}\{\left(e^{\mathrm{f}}\right)^2\} \geq J_{\tau^{\mathrm{f}}}^{-1}, \qquad \mathbb{E}\{\left(e^{\mathrm{b}}\right)^2\} \geq J_{\tau^{\mathrm{b}}}^{-1}. \tag{22}$$

C. PEB and OEB for RLP

To compute PEB and OEB, we first need the EFIM of the position and orientation, $\mathbf{J}_{\mathbf{o},\mathbf{p}}^{\mathrm{e,b}}$. However, $\mathbf{p}$ and $\mathbf{o}$ are functions of $\boldsymbol{\vartheta}$ and τ and, hence $\mathbf{J}_{\mathbf{o},\mathbf{p}}^{\mathrm{e,b}}$ can be obtained as a transformation of the EFIM of $\boldsymbol{\vartheta}$ and τ as outlined in Definition 1. Since the temporal and spatial parts in (18) are independent, the EFIM of $\boldsymbol{\vartheta}$ and τ is given by

$$\mathbf{J}_{\boldsymbol{\vartheta}\tau}^{\mathrm{e,b}} = \begin{bmatrix} \mathbf{J}_{\boldsymbol{\vartheta}}^{\mathrm{e,b}} & \mathbf{0}_4 \\ \mathbf{0}_4^{\mathrm{T}} & J_{\tau} \end{bmatrix}. \tag{23}$$

We now outline how to obtain $\mathbf{J}_{\boldsymbol{\vartheta}\tau}^{\mathrm{e,b}}$ before transforming it to obtain $\mathbf{J}_{\mathbf{o},\mathbf{p}}^{\mathrm{e,b}}$.

It is straight-forward from (19) that the EFIM of $\boldsymbol{\vartheta}$ based on the backward transmission is obtained using Schur complements as

$$\mathbf{J}_{\boldsymbol{\vartheta}}^{\mathrm{e,b}} = \mathbf{J}_{\boldsymbol{\vartheta}}^{\mathrm{b}} - \frac{1}{J_{\beta^{\mathrm{b}}}^{\mathrm{b}}}\mathbf{J}_{\boldsymbol{\vartheta}\beta^{\mathrm{b}}}^{\mathrm{b}}\left(\mathbf{J}_{\boldsymbol{\vartheta}\beta^{\mathrm{b}}}^{\mathrm{b}}\right)^{\mathrm{T}}. \tag{24}$$

According to (12), τ depends on the estimate of τ^{f} as well as the value of τ^{b}. While we can determine $J_{\tau^{\mathrm{f}}}$ based on $\mathbf{y}_2(t)$, $J_{\tau^{\mathrm{b}}}$ is based on $\mathbf{y}_1(t)$. Therefore, to obtain the FIM of τ rather than τ^{b} or τ^{f}, we apply the fact that, under RLP, the delays are not dependent on any of the other channel parameters. Towards that, recall that $\hat{\tau}^{\mathrm{b}} = 2\tau + e^{\mathrm{f}} + e^{\mathrm{b}} + \tau^{\mathrm{D}}$, and define

$$\tau' \triangleq \frac{\hat{\tau}^{\mathrm{b}} - \tau^{\mathrm{D}}}{2} = \tau + \frac{e^{\mathrm{f}} + e^{\mathrm{b}}}{2}. \tag{25}$$

Consequently, using (22) yields

$$\mathbb{E}\left\{\left(\tau' - \tau\right)^2\right\} \geq \frac{1}{4}\left(J_{\tau^{\mathrm{f}}}^{-1} + J_{\tau^{\mathrm{b}}}^{-1}\right), \tag{26}$$

that is,

$$J_\tau = 4\left(J_{\tau^{\mathrm{f}}}^{-1} + J_{\tau^{\mathrm{b}}}^{-1}\right)^{-1}. \tag{27}$$

Note that in this scenario, the estimation of τ is less accurate than the estimation of τ^{b} due to its further dependence of τ^{f}.

Applying Definition 1, to (23), it can be shown that

$$\mathbf{J}_{\mathbf{o},\mathbf{p}}^{\mathrm{e,b}}|_{\mathrm{RLP}} = \boldsymbol{\Upsilon}\mathbf{J}_{\boldsymbol{\vartheta}\tau}^{\mathrm{e,b}}\boldsymbol{\Upsilon}^{\mathrm{T}}, \tag{28}$$

where

$$\boldsymbol{\Upsilon} \triangleq \left[\begin{array}{cccc:c} \frac{\partial\theta_1}{\partial\mathbf{o}} & \frac{\partial\phi_1}{\partial\mathbf{o}} & \frac{\partial\theta_2}{\partial\mathbf{o}} & \frac{\partial\phi_2}{\partial\mathbf{o}} & \frac{\partial\tau}{\partial\mathbf{o}} \\ \frac{\partial\theta_1}{\partial\mathbf{p}} & \frac{\partial\phi_1}{\partial\mathbf{p}} & \frac{\partial\theta_2}{\partial\mathbf{p}} & \frac{\partial\phi_2}{\partial\mathbf{p}} & \frac{\partial\tau}{\partial\mathbf{p}} \end{array}\right] = \left[\boldsymbol{\Upsilon}_{\mathrm{s}} \vdots \boldsymbol{\Upsilon}_{\tau}\right]. \tag{29}$$

Consequently, for RLP, we can isolate the spatial and temporal parts and write,

$$\mathbf{J}_{\mathbf{o},\mathbf{p}}^{\mathrm{e,b}}|_{\mathrm{RLP}} = \underbrace{\boldsymbol{\Upsilon}_{\mathrm{s}}\mathbf{J}_{\boldsymbol{\vartheta}}^{\mathrm{e,b}}\boldsymbol{\Upsilon}_{\mathrm{s}}}_{\text{Spatial Part}} + \underbrace{J_\tau\boldsymbol{\Upsilon}_\tau\boldsymbol{\Upsilon}_\tau^{\mathrm{T}}}_{\text{Temporal Part}}. \tag{30}$$

The entries of $\boldsymbol{\Upsilon}_\tau$ and $\boldsymbol{\Upsilon}_{\mathrm{s}}^{\mathrm{b}}$ are easily obtained from the relations mapping from location parameters to channel parameters and can be found in [27], where it was concluded that $\boldsymbol{\Upsilon}_\tau$ is identical for the uplink and downlink, while $\boldsymbol{\Upsilon}_{\mathrm{s}}^{\mathrm{b}}$ is not. This results in an asymmetry in the spatial part of the FIM. To understand the implication of this asymmetry, we note that the UE position in the uplink is a function of the DOA and TOA, while in the downlink, it is a function of the DOD and TOA. However, DOD and DOA have different CRLBs, which means that the RLP localization performance in (30) depends on whether the localization is executed in the uplink (at BS) or downlink (at UE).

D. PEB and OEB for CLP

As can be inferred from (10), we have to retrieve B in CLP, in contrast to the RLP case. Therefore, we the vector of unknown parameters is

$$\boldsymbol{\varphi}_{\mathrm{C}} \triangleq \left[\boldsymbol{\vartheta}^{\mathrm{T}}, \psi^{\mathrm{b}}, \beta^{\mathrm{b}}, \psi^{\mathrm{f}}, \beta^{\mathrm{f}}, \tau, B\right]^{\mathrm{T}}. \tag{31}$$

To simplify the derivation, we treat the temporal parameters, (τ and B), in isolation of the spatial parameters ($\boldsymbol{\vartheta}^{\mathrm{T}}, \psi^{\mathrm{b}}, \beta^{\mathrm{b}}, \psi^{\mathrm{f}}, \beta^{\mathrm{f}}$) because both sets are independent. Similar to (23), we seek to compute

$$\mathbf{J}_{\boldsymbol{\vartheta}\tau}^{\mathrm{e}} \triangleq \begin{bmatrix} \mathbf{J}_{\boldsymbol{\vartheta}}^{\mathrm{e}} & \mathbf{0}_4 \\ \mathbf{0}_4^{\mathrm{T}} & J_\tau^{\mathrm{e}} \end{bmatrix}, \tag{32}$$

where $\mathbf{J}_{\boldsymbol{\vartheta}}^{\mathrm{e}}$ is to be computed from FIM of the spatial parameters and J_τ^{e} is to be computed from the temporal ones.

Since D_2 transmission time is independent of the TOA of $\mathbf{y}_2(t)$, the two transmissions occur in non-overlapping time slots, and the noise is independent at both sides, the forward and backward transmissions can be considered independent. Therefore, the FIMs can be added according to the following Theorem.

Theorem 1: Consider a random process to observe the unknown parameter $\mathbf{x}$ along with the unknown nuisance parameter $\mathbf{z}_1$. Consider also another random process to observe $\mathbf{x}$ along with the unknown nuisance parameter $\mathbf{z}_2$. If both processes are independent and $\mathbf{z}_1$ and $\mathbf{z}_2$, are independent, then total EFIM of $\mathbf{x}$ is

$$\mathbf{J}_{\mathbf{x}}^{\mathrm{e}} = \mathbf{J}_{\mathbf{x}}^{\mathrm{e},1} + \mathbf{J}_{\mathbf{x}}^{\mathrm{e},2}, \tag{33}$$

where $\mathbf{J}_{\mathbf{x}}^{\mathrm{e,i}}$ is the EFIM of $\mathbf{x}$ obtained from the i-th process.

Proof: See Appendix B. ■

In other words, the EFIM of $\boldsymbol{\vartheta}$ can be written as $\mathbf{J}_{\boldsymbol{\vartheta}}^{\mathrm{e}} = \mathbf{J}_{\boldsymbol{\vartheta}}^{\mathrm{e,b}} + \mathbf{J}_{\boldsymbol{\vartheta}}^{\mathrm{e,f}}$ by summing the EFIMs of $\boldsymbol{\vartheta}$ computed from $\mathbf{y}_1(t)$ and $\mathbf{y}_2(t)$. From (19), it follows that

$$\mathbf{J}_{\boldsymbol{\vartheta}}^{\mathrm{e}} = \mathbf{J}_{\boldsymbol{\vartheta}}^{\mathrm{b}} + \mathbf{J}_{\boldsymbol{\vartheta}}^{\mathrm{f}} - \frac{1}{J_{\beta^{\mathrm{b}}}^{\mathrm{b}}}\mathbf{J}_{\boldsymbol{\vartheta}\beta^{\mathrm{b}}}^{\mathrm{b}}\left(\mathbf{J}_{\boldsymbol{\vartheta}\beta^{\mathrm{b}}}^{\mathrm{b}}\right)^{\mathrm{T}} - \frac{1}{J_{\beta^{\mathrm{f}}}^{\mathrm{f}}}\mathbf{J}_{\boldsymbol{\vartheta}\beta^{\mathrm{f}}}^{\mathrm{f}}\left(\mathbf{J}_{\boldsymbol{\vartheta}\beta^{\mathrm{f}}}^{\mathrm{f}}\right)^{\mathrm{T}}.$$

Moreover, J_τ^{e} can be obtained noting that in the backward transmission $\tau^{\mathrm{b}} = t^{\mathrm{b}} + \tau - B$, while in the forward transmission $\tau^{\mathrm{f}} = \tau + B$, and that τ is independent of any other parameters. Hence, using the transformation of parameters and the fact that the two transmissions are independent, we can write the FIM of $[\tau, B]^{\mathrm{T}}$ as

$$\mathbf{J}_{\tau B} = J_{\tau^{\mathrm{b}}}\begin{bmatrix} 1 & -1 \\ -1 & 1 \end{bmatrix} + J_{\tau^{\mathrm{f}}}\begin{bmatrix} 1 & 1 \\ 1 & 1 \end{bmatrix} \tag{34}$$

from which EFIM of τ is obtained by Schur complement as

$$J_\tau^{\mathrm{e}} = 4\left(J_{\tau^{\mathrm{f}}}^{-1} + J_{\tau^{\mathrm{b}}}^{-1}\right)^{-1}. \tag{35}$$

It is interesting to see that the temporal information represented by J_τ is identical for both CLP (35) and RLP (27). Therefore, any performance difference between these two protocols is attributed to the spatial information only.

We now derive the EFIM of the position and orientation. Based on (32) and Definition 2

$$\begin{aligned}\mathbf{J}_{\mathbf{o},\mathbf{p}}^{\mathrm{e}}|_{\mathrm{CLP}} &= \boldsymbol{\Upsilon}\mathbf{J}_{\boldsymbol{\vartheta}\tau}^{\mathrm{e}}\boldsymbol{\Upsilon}^{\mathrm{T}}, \\ &= \underbrace{\boldsymbol{\Upsilon}_{\mathrm{s}}\mathbf{J}_{\boldsymbol{\vartheta}}^{\mathrm{e,f}}\boldsymbol{\Upsilon}_{\mathrm{s}}^{\mathrm{T}}}_{\text{Forward Spatial Part}} + \underbrace{\boldsymbol{\Upsilon}_{\mathrm{s}}\mathbf{J}_{\boldsymbol{\vartheta}}^{\mathrm{e,b}}\boldsymbol{\Upsilon}_{\mathrm{s}}^{\mathrm{T}}}_{\text{Backward Spatial Part}} + \underbrace{J_\tau\boldsymbol{\Upsilon}_\tau\boldsymbol{\Upsilon}_\tau^{\mathrm{T}}}_{\text{Temporal Part}}.\end{aligned} \tag{36}$$

Note that (36) comprises three terms: two terms related to the spatial information in the forward and backward transmissions, and one term related to the temporal information.

E. Performance Comparison of RLP, CLP, and OWL

The EFIM of position and orientation under RLP is given in (30), while that under CLP is given in (36). In this section, we compare the performance of these two protocols with the standard one-way localization (OWL) from [27], where it was shown that

$$\mathbf{J}_{\mathbf{o},\mathbf{p}}^{\mathrm{e,b}}|_{\mathrm{OWL}} = \underbrace{\boldsymbol{\Upsilon}_{\mathrm{s}}\mathbf{J}_{\boldsymbol{\vartheta}}^{\mathrm{e,b}}\boldsymbol{\Upsilon}_{\mathrm{s}}^{\mathrm{T}}}_{\text{Spatial Part}} + \underbrace{J_{\tau^{\mathrm{b}}}\boldsymbol{\Upsilon}_\tau\boldsymbol{\Upsilon}_\tau^{\mathrm{T}}}_{\text{Temporal Part}}, \tag{37}$$

under the assumption of perfect synchronization between the two devices (i.e., $B = 0$).

1) RLP vs. CLP: Comparing RLP to CLP, we note that (30) contains only one spatial information term, related to the backward transmission, and another temporal information term. These two terms are equal to their counterparts in (36). Hence,

$\mathbf{J}^{\mathrm{e}}_{\mathbf{o},\mathbf{p}}|_{\mathrm{CLP}} \succ \mathbf{J}^{\mathrm{e,b}}_{\mathbf{o},\mathbf{p}}|_{\mathrm{RLP}}$, meaning that CLP will always outperform RLP. Nevertheless, CLP requires additional overhead, as it involves sending back the waveform $\mathbf{y}_2(t)$ to D_1 (or estimated parameters with uncertainty) and thus requires an additional data transmission.

2) RLP vs. OWL: Inspecting (37), it can be seen that $\mathbf{J}^{\mathrm{e,b}}_{\mathbf{o},\mathbf{p}}|_{\mathrm{OWL}}$ has the same expression as (30), but with

$$J_\tau = J_{\tau^{\mathrm{b}}}. \tag{38}$$

This means the both RLP and OWL have the same spatial information but differ in the temporal information. However, it is not clear which protocol is superior. Therefore, we provide the following proposition.

Proposition 1: RLP outperforms OWL if $J_{\tau^{\mathrm{f}}} > \frac{1}{3} J_{\tau^{\mathrm{b}}}$.

Proof: Comparing RLP with OWL, it can be seen that they have equal spatial, but different temporal information. Comparing (27) with (38), for RLP to outperform OWL, we should have

$$J_{\tau^{\mathrm{b}}} < 4\left(J^{-1}_{\tau^{\mathrm{f}}} + J^{-1}_{\tau^{\mathrm{b}}}\right)^{-1} = J_{\tau^{\mathrm{b}}} \frac{4 J_{\tau^{\mathrm{f}}}}{J_{\tau^{\mathrm{f}}} + J_{\tau^{\mathrm{b}}}},$$

which leads to $J_{\tau^{\mathrm{f}}} > \frac{1}{3} J_{\tau^{\mathrm{b}}}$. ■

This means that, when the bandwidth is equal in both directions, the forward link should have at least one third the signal-to-noise ratio (SNR) of the backward link for RLP to outperform OWL. From (43q), it can be seen that this mainly depends on the transmit and receive beamforming. However, under the general case of non-identical bandwidth allocation, (43q) can be used to determine the values of bandwidth and SNR that satisfy the condition in Proposition 1.

F. Relationship of RLP and CLP With Channel Parameters

Since the derived position and orientation bounds are obtained through transforming the channel parameter bounds, the localization performance is ultimately affected by the channel parameter estimation accuracy. In [27], it was concluded that the squared PEB is the sum of the CRLBs of TOA and the BS angle (DOA in the uplink or DOD in the downlink). It was also concluded that the CRLB of DOA is better than the CRLB of DOD. Extending these results to the RLP and CLP in this paper, it can be seen that from (30), the RLP performance is governed by the backward transmission from D_2 to D_1. In other words, if the backward transmission is uplink, D_1 is a BS, whose angle is a DOA, which leads to a better PEB. Note that in such a case, DOD estimation error does not affect the localization performance. The opposite is true if D_1 is a UE.

For CLP, it can be seen that from (36) that the squared PEB is the sum of the CRLB of DOA, DOD and TOA, meaning that regardless of the BS and UE roles, the PEB is affected by the error of estimating all of these three parameters.

The squared OEB is the sum of the CRLBs of DOA and DOD [27], and hence it is not affected by the accuracy of the TOA estimation.

G. Insights on NLOS

When the signal propagation occurs in mixed propagation environment (LOS and NLOS), the delay of the LOS path, being the first and strongest path, can still be separated and identified, while the delays of NLOS paths must be subsequently estimated. For RLP, the NLOS paths in the backward transmission can assist the positioning, as shown in [27]. On the other hand, for CLP, the parameters of the NLOS paths in the forward and backward transmissions can be estimated separately. However, this will give rise to a path association problem, whereby the set of parameters estimated from the forward transmission have to be paired with their counter parts in the backward transmission and with the scatterers or reflectors in the environment to re-establish the different paths. Moreover, when the LOS is obstructed, the localization performance is severely degraded [36].

V. Simulation Results and Discussion

A. Simulation Environment

1) System Layout and Channel: In our simulations, we investigate and compare the RLP and CLP using the position and orientation error bounds to quantify the estimation accuracy. Since both protocols involve forward and backward transmission, we selected an equal number of antennas at both the BS and the UE to make the comparison of these protocols fair.[7] Towards that, we consider a BS and a UE both with 12×12 uniform rectangular antenna array (URA) communicating via a LOS. Moreover, we assume that the BS array is located in the xz-plane centered about the origin $[0, 0, 0]^{\mathrm{T}}$, thus has orientation angles of $[0^\circ, 0^\circ]^{\mathrm{T}}$. On the other hand, the UE moves freely within a diamond-shape 120° defined by the vertices $\{(0, 0, -10), (25\sqrt{3}, 25, -10), (0, 50, -10), (-25\sqrt{3}, 25, -10)\}$. That is, the BS height is 10 meters. We focus on two cases of orientation angles with respect to the z-axis and x-axis: $\mathbf{o} = [\chi_0, \zeta_0] = [0^\circ, 0^\circ]^{\mathrm{T}}$ and $\mathbf{o} = [30^\circ, 30^\circ]^{\mathrm{T}}$ as specified in the context. Finally, at a distance d_1, the channel gain is modeled as $\beta^{\mathrm{b}} = \beta^{\mathrm{f}} = \frac{\lambda}{4\pi d_1}$ [38].

2) Transmit-Receive Model: We select the mmWave frequency of $f = 38$ GHz, and bandwidth,[8] $W = 125$ MHz. We assume an ideal sinc pulse-shaping filter such that $W^2_{\mathrm{eff}} = W^2/3$. The transmitted power $E_{\mathrm{t}}/T_{\mathrm{s}} = 0$ dBm, and $N_0 = -170$ dBm/Hz. Furthermore, we specify the number of pilots to be $N_{\mathrm{s}} = 64$ pilot symbols. This yields a location-dependent SNR of

$$\mathrm{SNR}\ [\mathrm{dB}] = 150.26 + 20\log_{10}\left(\beta^{\mathrm{b}} \|\mathbf{a}_i^{\mathrm{T}} \mathbf{F}_i^{\mathrm{H}}\| \|\mathbf{W}_j^{\mathrm{H}} \mathbf{a}_j\|\right), \tag{39}$$

where $i, j \in \{1, 2\}, i \neq j$, specified depending on the communication direction being forward or backward. Note that this SNR results from beamforming gain of all the N_{B_1} and N_{B_2} beams combined. Although our formulation holds for any type

[7] It is understood that BSs can accommodate more complexity, and its array can have a larger size, such as that in [24] where 10,000 antennas are used. However, we use an equal number of antennas on D_1 and D_2 in order to explore the intrinsic differences between the protocols. These differences result from the lack of symmetry between the two links because the orientation is only known for one device but not the other. Thus, we prevent masking our protocol analysis by using the same number of antennas.

[8] At these frequency and bandwidth values, beam squint is negligible. From [39] pointing error due to beam squint is proportional to $(1 + f/W)^{-1} \approx 1$.

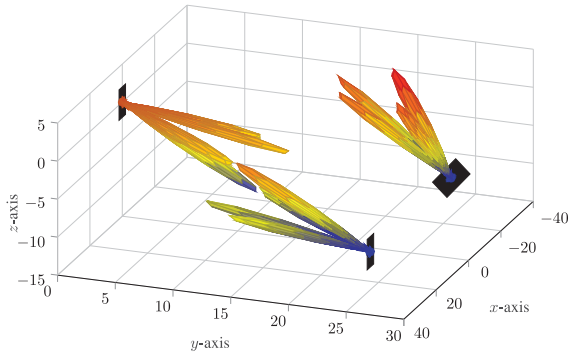

Fig. 4. Beamforming example with 4 beams. The rightmost device has orientation angles of 30°, while the other two have 0°.

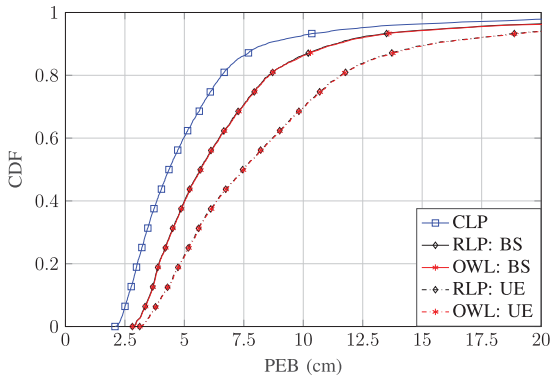

Fig. 5. CDF of PEB with UE orientation angles of 0°, and $N_{\mathrm{UE}} = N_{\mathrm{BS}} = 144$, $N_{\mathrm{B}} = 25$.

of analog beamforming, in our numerical simulations, we adopt *fixed* directional beamforming as an example scheme similar to [27]. We consider $1 \leq b \leq N_{\mathrm{B}_1} = N_{\mathrm{B}_2} = 25$ beams at both the UE and BS, such that

$$\mathbf{f}_{1,b} = \frac{1}{\sqrt{N_{\mathrm{B}_1}}}\mathbf{a}_1(\theta^{\mathrm{f}}_{1,b}, \phi^{\mathrm{f}}_{1,b}),$$

$$\mathbf{w}_{1,b} = \frac{1}{\sqrt{N_{\mathrm{B}_1}}}\mathbf{a}_1(\theta^{\mathrm{w}}_{1,b}, \phi^{\mathrm{w}}_{1,b}),$$

are D_1 transmit and receive beams pointing towards $(\theta^{\mathrm{f}}_{1,b}, \phi^{\mathrm{f}}_{1,b})$ and $(\theta^{\mathrm{w}}_{1,b}, \phi^{\mathrm{w}}_{1,b})$, respectively. The directions of the beams at the BS are chosen to be equispaced on the sector. On the UE, these directions are reversed to point upwards and rotated with respect to the UE frame of reference by the same orientation angles specified in the studied experiment. This setting provides 90% of the locations with an SNR of at least 17 dB. Fig. 4 provides three examples on beamforming configuration: a BS at (0, 0, 0), with beams pointing downwards, a UE at $(25, 25, -10)$ with zero orientation angles, and another UE at $(-25, 25, -10)$ with $\mathbf{o} = [30^\circ, 30^\circ]^{\mathrm{T}}$. The black rectangles denote the array frame of reference of the device. Note that the first UE has reversed beam direction compared to BS, while the second UE has beam directions reversed and rotated by $[30^\circ, 30^\circ]^{\mathrm{T}}$, so that the beam directions remain constant with respect to the UE local frame of reference.

3) Scenarios Studied: We study the PEB and OEB under RLP and CLP and compare these bounds to those obtained for OWL in [27]. Each of these three protocols is studied when localization is performed in the uplink (at BS) and in the downlink (at UE). Recall that CLP is symmetric in both cases, hence only one curve is given.

B. PEB and OEB With 0° UE Orientation

The cumulative distribution function (CDF) of the PEB with zero orientation angles is provided in Fig. 5 for all the considered protocols. First of all, to have a fair comparison, we compare the three solid curves corresponding to uplink localization, and then compare those related to downlink localization (dash-dot lines). It can be seen that RLP provides a negligible improvement over OWL. Despite that, RLP is still a better approach since it alleviates the need for high-accuracy synchronization, with the cost of UE-BS coordination. As discussed in Section IV-E, RLP and OWL have the same spatial component, but RLP has higher temporal information content. However, Fig. 5 shows almost identical results for both protocols, which means that the additional temporal information in RLP is of little importance, and thus the localization performance is limited by the angles estimation rather than the time delay. To understand this phenomenon more, we study the impact of the bandwidth on the performance later in Section V-D. On the other hand, as expected, CLP represents the best approach among the three studied, since it attains more useful information. However, this requires a more complex implementation due to the need for a feedback channel.

Comparing the dash-dotted curves with the solid curves in Fig. 5, it can be seen that the three protocols behave in the downlink in a manner similar to the uplink. And, it can also be seen that while OWL and RLP are almost identical, CLP is superior to both. However, the reasons why the performance of RLP and OWL is worse in the downlink are beyond the scope of this paper and were extensively studied in [27]. Briefly, it was concluded that, under matched orientation between the BS and UE, the uplink PEB is better than the downlink PEB. This is because 1) PEB is a function of the CRLB of the BS angles, and 2) CRLB of DOA is lower than CRLB of DOD. Therefore, when the BS angles are DOAs (uplink), the PEB will be lower.

Considering the CDF of the OEB with zero orientation angles in Fig. 6, it can be seen that RLP and OWL exhibit identical performance. Note that OEB depends on DOA and DOD, while the enhancement of RLP over OWL is in the temporal domain. Furthermore, in line with the results in [27] with zero orientation angles, the uplink and downlink OEB are the same. Therefore, the four curves of RLP and OWL with uplink and downlink localization coincide. Moreover, in terms of OEB, CLP is also better than RLP and OWL due to the fourth term in (36), which accounts for the coupling between the path gain and the transmission angles, providing more spatial information on the orientation angles. Intuitively, this higher information is a result of estimating the path gain in both transmissions.

C. PEB and OEB With 30° UE Orientation

The CDF of the PEB with orientation angles $\mathbf{o} = [30^\circ, 30^\circ]^{\mathrm{T}}$ is shown in Fig. 7, for all the considered protocols. The overall observation from this figure, in comparison to Fig. 5, is that

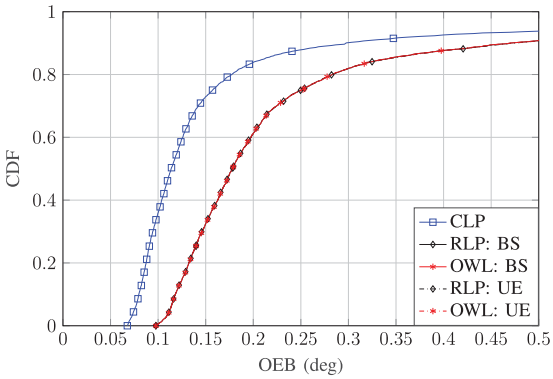

Fig. 6. CDF of OEB with UE orientation angles of 0°, and $N_{\mathrm{UE}} = N_{\mathrm{BS}} = 144$, $N_{\mathrm{B}} = 25$.

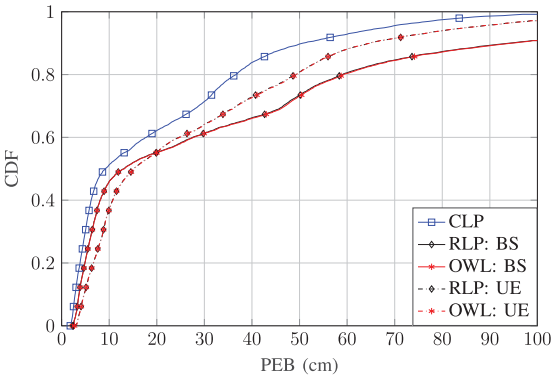

Fig. 7. CDF of PEB with UE orientation angles of 30°, and $N_{\mathrm{UE}} = N_{\mathrm{BS}} = 144$, $N_{\mathrm{B}} = 25$.

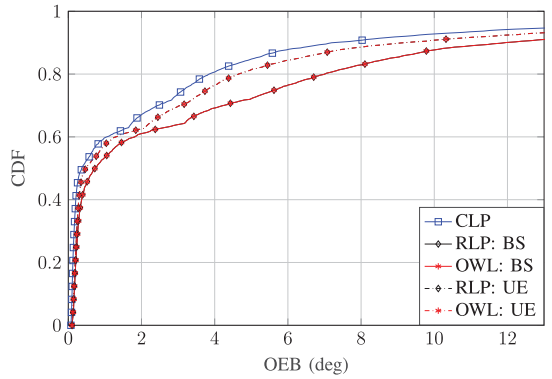

Fig. 8. CDF of OEB with UE orientation angles of 30°, and $N_{\mathrm{UE}} = N_{\mathrm{BS}} = 144$, $N_{\mathrm{B}} = 25$.

the performance worsens when the beams are steered away, i.e., when the orientation angles are non-zero. This can result in a loss of beamforming gain that depends non-linearly on the UE location and orientation angles. However, CLP performance is still superior to RLP and OWL. In this example, performance loss of 42 cm, 54 cm, and 80 cm were observed at a PEB CDF of 90%, under CLP, uplink RLP, and downlink RLP, respectively. On the other hand, comparing Fig. 8 with Fig. 6, it can be seen that, at a CDF of 90%, there is an OEB performance loss of 6.8°, 8.8°, and 11.5° under CLP, uplink RLP, and downlink

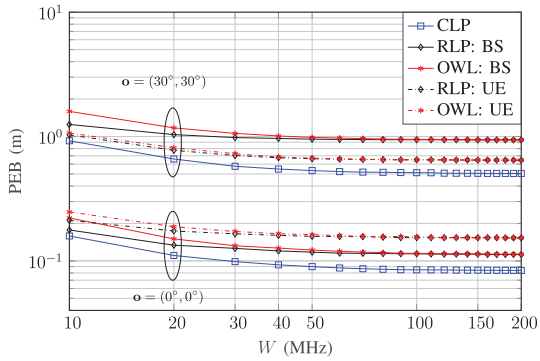

Fig. 9. PEB at 0.9 CDF with respect to the bandwidth W.

RLP, respectively. Considering the PEB and OEB loss, it can be concluded that, among the studied approaches, CLP is the approach that is most robust to UE mis-orientation. Finally, we note that in comparison to the case of matched orientation, under 30° mis-orientation, the system can still provide sub-meter PEB, while providing significantly higher OEB. This means that orientation estimation is more challenging than position estimation. Recall that orientation changes the beamforming angles, which impacts localization performance. Hence, the study of orientation in this context is meaningful, despite this degraded performance.

D. Impact of the System Bandwidth on PEB

In Section V-C, we concluded that the system is limited by the estimation of the angles rather than the time delay. To investigate this phenomenon further, we now look closer into the impact of the bandwidth. In the context of localization and ranging, higher bandwidths provide a more accurate estimation of the TOA, which leads to better localization bounds in general. Towards that, the results in Fig. 9 indicate that as the bandwidth increases, the PEB decreases, until it reaches a floor at around 100 MHz when $\mathbf{o} = [0°, 0°]^{\mathrm{T}}$, and 60 MHz when $\mathbf{o} = [30°, 30°]^{\mathrm{T}}$. Based on these results, we make the following observations:

1) At higher bandwidths that are more relevant in mmWave, the temporal information is very high compared to the spatial information, and the performance becomes fixed with W, i.e., the systems are spatially-limited.
2) Under mis-orientation, the accuracy of spatial information degrades, and the system becomes spatially-limited. Hence, the improved temporal information does not provide any benefit to the performance achieved at lower bandwidths.
3) On the contrary, for lower bandwidths, the amount of temporal information decreases and becomes comparable to the spatial information. Therefore, the weight of the temporal information in the forward transmission becomes more significant, and the difference between OWL and RLP becomes more pronounced.

E. Impact of N_{BS} and N_{UE} on PEB

We now study the effect of the number of antennas at BS and UE on the PEB under CLP and RLP. Since this number can be

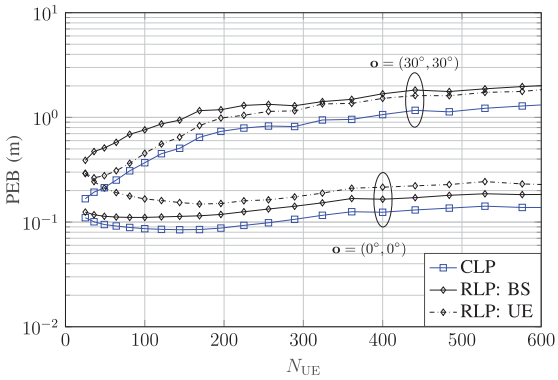

Fig. 10. PEB at 0.9 CDF as a function of the UE number of antennas, with $N_{\mathrm{B}} = 25$, with orientation angles 0° and 30°, and $N_{\mathrm{BS}} = 144$.

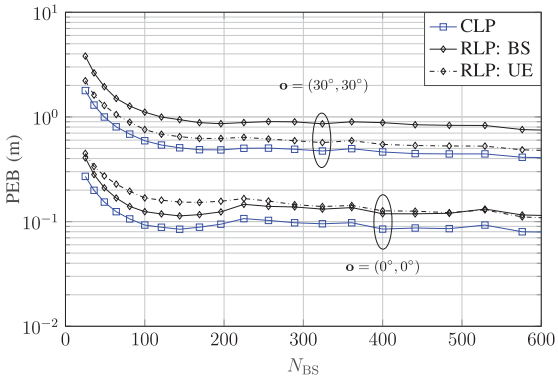

Fig. 11. PEB at 0.9 CDF as a function of the BS number of antennas, with $N_{\mathrm{B}} = 25$, with orientation angles 0° and 30°, and $N_{\mathrm{UE}} = 144$.

N_1 or N_2 depending on the device role, we use N_{BS} and N_{UE} to unify the notation of the number of antennas at BS and UE, respectively.

Fig. 10 illustrates the effect of N_{UE} on PEB with $N_{\mathrm{B}} = 25$ and $N_{\mathrm{BS}} = 144$. It can be seen that at matched orientation (0°, 0°), performance tends to slightly improve with low to moderate N_{UE} values. However, higher N_{UE} generally results in a worse performance. This is because with higher N_{UE}, the UE beams become narrower, and more beams are required to provide a full area coverage. It can also be noticed that, with an orientation of (30°, 30°), the rate of performance deterioration is higher. It is interesting to see that this rate is almost the same for the three protocols, which means that the performance loss is mainly due to SNR loss.

On the other hand, the impact of N_{BS} is shown in Fig. 11 with $N_{\mathrm{B}} = 25$ and $N_{\mathrm{UE}} = 144$. It can be seen that a higher N_{BS} slightly improves the PEB in general. Similar to the case in Fig. 10, it is understood that the PEB will generally increase when N_{BS} is arbitrarily large, albeit, at N_{BS} values well beyond those displayed in Fig. 11, and with a lesser magnitude than higher N_{UE}. Therefore, adding more antennas at the BS will not reduce the localization performance, as the UE antennas potentially would, at least within the studied range of array size. Finally, notice that both Figs. 10 and 11 exhibit some non-monotonic trend. This is due to the nature of directional beamforming, whereby the beamforming gain depends on the user location, number of antennas, and beams directions as detailed in [40]. In other words, varying the number of antennas results in a different sidelobe pattern that non-linearly varies the PEB and OEB.

VI. Conclusion

Many publications on localization assume that the BS and UE are tightly synchronized. However, usually, communication systems are not synchronized to a high-level useful for localization. Focusing on this issue, in this paper, we considered two protocols of two-way localization referred to round-trip localization protocol (RLP) and collaborative localization protocol (CLP). We investigated the PEB and OEB under these two protocols, where we showed mathematically that CLP outperforms RLP with a significant margin. However, this comes with the cost of requiring a feedback channel, unlike RLP where no synchronization or feedback are required, although it may need dedicated hardware to trigger the response. In our derivations, we considered beamforming at the transmitter and the receiver and accounted for the spatially-correlated receive noise. Considering the results of the numerical simulation, the enhancement observed for RLP over the traditional OWL was limited. That is, the localization was angle-limited rather than delay-limited. Moreover, our numerical results also showed that it is more beneficial to have more antennas at the BS than at the UE.

Future work based on this paper includes considering adaptive beamforming, whereby the beam directions are modified in the second round of transmission. Moreover, multipath propagation would be a relevant extension, since scatterers may differ in the uplink and downlink, depending on the beam directions.

Appendix A
Derivation of the Elements of the FIM of the Channel Parameters

Consider backward transmission round. In this case, D_1 has the following observation

$$\mathbf{y}_1(t) = \sqrt{N_1 N_2 E_{\mathrm{t}}} h^{\mathrm{b}} \mathbf{W}_1^{\mathrm{H}} \mathbf{a}_1 \mathbf{a}_2^{\mathrm{T}} \mathbf{F}_2 \mathbf{s}_2(t - \tau^{\mathrm{b}}) + \mathbf{n}_1(t). \quad (40)$$

For the case of zero-mean additive correlated Gaussian noise, the FIM of $\boldsymbol{\varphi}^{\mathrm{b}}$ is given by [37]

$$J_{xy}^{\mathrm{b}} \triangleq = \frac{1}{N_0} \int_0^{T_{\mathrm{o}}} \Re \left\{ \frac{\partial \boldsymbol{\mu}^{\mathrm{H}}(t)}{\partial x} \left(\mathbf{W}_1^{\mathrm{H}} \mathbf{W}_1 \right)^{-1} \frac{\partial \boldsymbol{\mu}(t)}{\partial y} \right\} \mathrm{d}t,$$
$$x, y \in \{\theta_1, \phi_1, \theta_2, \phi_2, \psi^{\mathrm{b}}, \beta^{\mathrm{b}}, \tau^{\mathrm{b}}\} \quad (41)$$

where $\boldsymbol{\mu}(t)$ is the mean of the observation vector, and T_{o} is assumed to be long enough to receive the entire pilot signal. Consequently, we write

$$\boldsymbol{\mu}(t) = \sqrt{N_1 N_2 E_{\mathrm{t}}} \beta^{\mathrm{b}} \mathrm{e}^{j\psi^{\mathrm{b}}} \mathbf{W}_1^{\mathrm{H}} \mathbf{a}_1 \mathbf{a}_2^{\mathrm{T}} \mathbf{F}_2 \mathbf{s}_2(t - \tau^{\mathrm{b}}). \quad (42)$$

Defining $\dot{\mathbf{s}}(t) \triangleq \frac{\partial \mathbf{s}(t)}{\partial t}$, $\mathbf{k}_{\mathrm{i}} = \frac{\partial}{\partial \theta_i} \mathbf{a}_{\mathrm{i}}$, $\mathbf{p}_{\mathrm{i}} = \frac{\partial}{\partial \phi_i} \mathbf{a}_{\mathrm{i}}$, $i \in \{1, 2\}$, and the operator $\mathbf{P}_{\mathbf{A}} \triangleq \mathbf{A}(\mathbf{A}^{\mathrm{H}}\mathbf{A})^{-1}\mathbf{A}^{\mathrm{H}}$, and $\gamma \triangleq N_1 N_2 N_{\mathrm{s}} E_{\mathrm{t}} / N_0$,

we can write the following

$$J^{\mathrm{b}}_{\theta_1} = \gamma\beta^{\mathrm{b}^2}\left(\mathbf{a}_2^{\mathrm{T}}\mathbf{F}_2\mathbf{F}_2^{\mathrm{H}}\mathbf{a}_2^*\right)\left(\mathbf{k}_1^{\mathrm{H}}\mathbf{P}_{\mathbf{W}_1}\mathbf{k}_1\right) \tag{43a}$$

$$J^{\mathrm{b}}_{\phi_1} = \gamma\beta^{\mathrm{b}^2}\left(\mathbf{a}_2^{\mathrm{T}}\mathbf{F}_2\mathbf{F}_2^{\mathrm{H}}\mathbf{a}_2^*\right)\left(\mathbf{p}_1^{\mathrm{H}}\mathbf{P}_{\mathbf{W}_1}\mathbf{p}_1\right) \tag{43b}$$

$$J^{\mathrm{b}}_{\theta_2} = \gamma\beta^{\mathrm{b}^2}\left(\mathbf{k}_2^{\mathrm{T}}\mathbf{F}_2\mathbf{F}_2^{\mathrm{H}}\mathbf{k}_2^*\right)\left(\mathbf{a}_1^{\mathrm{H}}\mathbf{P}_{\mathbf{W}_1}\mathbf{a}_1\right) \tag{43c}$$

$$J^{\mathrm{b}}_{\phi_2} = \gamma\beta^{\mathrm{b}^2}\left(\mathbf{p}_2^{\mathrm{T}}\mathbf{F}_2\mathbf{F}_2^{\mathrm{H}}\mathbf{p}_2^*\right)\left(\mathbf{a}_1^{\mathrm{H}}\mathbf{P}_{\mathbf{W}_1}\mathbf{a}_1\right) \tag{43d}$$

$$J^{\mathrm{b}}_{\beta^{\mathrm{b}}} = \gamma\left(\mathbf{a}_2^{\mathrm{T}}\mathbf{F}_2\mathbf{F}_2^{\mathrm{H}}\mathbf{a}_2^*\right)\left(\mathbf{a}_1^{\mathrm{H}}\mathbf{P}_{\mathbf{W}_1}\mathbf{a}_1\right), \tag{43e}$$

$$J^{\mathrm{b}}_{\psi^{\mathrm{b}}} = \gamma\beta^{\mathrm{b}^2}\left(\mathbf{a}_2^{\mathrm{T}}\mathbf{F}_2\mathbf{F}_2^{\mathrm{H}}\mathbf{a}_2^*\right)\left(\mathbf{a}_1^{\mathrm{H}}\mathbf{P}_{\mathbf{W}_1}\mathbf{a}_1\right), \tag{43f}$$

$$J^{\mathrm{b}}_{\theta_1\phi_1} = \gamma\beta^{\mathrm{b}^2}\left(\mathbf{a}_2^{\mathrm{T}}\mathbf{F}_2\mathbf{F}_2^{\mathrm{H}}\mathbf{a}_2^*\right)\left(\mathbf{p}_1^{\mathrm{H}}\mathbf{P}_{\mathbf{W}_1}\mathbf{k}_1\right), \tag{43g}$$

$$J^{\mathrm{b}}_{\theta_1\theta_2} = \gamma\beta^{\mathrm{b}^2}\left(\mathbf{k}_2^{\mathrm{T}}\mathbf{F}_2\mathbf{F}_2^{\mathrm{H}}\mathbf{a}_2^*\right)\left(\mathbf{k}_1^{\mathrm{H}}\mathbf{P}_{\mathbf{W}_1}\mathbf{a}_1\right), \tag{43h}$$

$$J^{\mathrm{b}}_{\theta_1\phi_2} = \gamma\beta^{\mathrm{b}^2}\left(\mathbf{p}_2^{\mathrm{T}}\mathbf{F}_2\mathbf{F}_2^{\mathrm{H}}\mathbf{a}_2^*\right)\left(\mathbf{k}_1^{\mathrm{H}}\mathbf{P}_{\mathbf{W}_1}\mathbf{a}_1\right), \tag{43i}$$

$$J^{\mathrm{b}}_{\theta_1\beta^{\mathrm{b}}} = \gamma\beta^{\mathrm{b}}\left(\mathbf{a}_2^{\mathrm{T}}\mathbf{F}_2\mathbf{F}_2^{\mathrm{H}}\mathbf{a}_2^*\right)\left(\mathbf{k}_1^{\mathrm{H}}\mathbf{P}_{\mathbf{W}_1}\mathbf{a}_1\right) \tag{43j}$$

$$J^{\mathrm{b}}_{\phi_1\theta_2} = \gamma\beta^{\mathrm{b}^2}\left(\mathbf{k}_2^{\mathrm{T}}\mathbf{F}_2\mathbf{F}_2^{\mathrm{H}}\mathbf{a}_2^*\right)\left(\mathbf{p}_1^{\mathrm{H}}\mathbf{P}_{\mathbf{W}_1}\mathbf{a}_1\right), \tag{43k}$$

$$J^{\mathrm{b}}_{\phi_1\phi_2} = \gamma\beta^{\mathrm{b}^2}\left(\mathbf{p}_2^{\mathrm{T}}\mathbf{F}_2\mathbf{F}_2^{\mathrm{H}}\mathbf{a}_2^*\right)\left(\mathbf{p}_1^{\mathrm{H}}\mathbf{P}_{\mathbf{W}_1}\mathbf{a}_1\right), \tag{43l}$$

$$J^{\mathrm{b}}_{\phi_1\beta^{\mathrm{b}}} = \gamma\beta^{\mathrm{b}}\left(\mathbf{a}_2^{\mathrm{T}}\mathbf{F}_2\mathbf{F}_2^{\mathrm{H}}\mathbf{a}_2^*\right)\left(\mathbf{p}_1^{\mathrm{H}}\mathbf{P}_{\mathbf{W}_1}\mathbf{a}_1\right), \tag{43m}$$

$$J^{\mathrm{b}}_{\theta_2\phi_2} = \gamma\beta^{\mathrm{b}^2}\left(\mathbf{p}_2^{\mathrm{T}}\mathbf{F}_2\mathbf{F}_2^{\mathrm{H}}\mathbf{k}_2^*\right)\left(\mathbf{a}_1^{\mathrm{H}}\mathbf{P}_{\mathbf{W}_1}\mathbf{a}_1\right), \tag{43n}$$

$$J^{\mathrm{b}}_{\theta_2\beta^{\mathrm{b}}} = \gamma\beta^{\mathrm{b}}\left(\mathbf{a}_2^{\mathrm{T}}\mathbf{F}_2\mathbf{F}_2^{\mathrm{H}}\mathbf{k}_2^*\right)\left(\mathbf{a}_1^{\mathrm{H}}\mathbf{P}_{\mathbf{W}_1}\mathbf{a}_1\right), \tag{43o}$$

$$J^{\mathrm{b}}_{\phi_2\beta^{\mathrm{b}}} = \gamma\beta^{\mathrm{b}}\left(\mathbf{a}_2^{\mathrm{T}}\mathbf{F}_2\mathbf{F}_2^{\mathrm{H}}\mathbf{p}_2^*\right)\left(\mathbf{a}_1^{\mathrm{H}}\mathbf{P}_{\mathbf{W}_1}\mathbf{a}_1\right), \tag{43p}$$

$$J_{\tau^{\mathrm{b}}} = 4\gamma\beta^{\mathrm{b}^2}\pi^2 W_{\mathrm{eff}}^2\left(\mathbf{a}_2^{\mathrm{T}}\mathbf{F}_2\mathbf{F}_2^{\mathrm{H}}\mathbf{a}_2^*\right)\left(\mathbf{a}_1^{\mathrm{H}}\mathbf{P}_{\mathbf{W}_1}\mathbf{a}_1\right). \tag{43q}$$

where

$$W_{\mathrm{eff}}^2 = \int_{-W/2}^{W/2} f^2|G(f)|^2\mathrm{d}f.$$

Other entries in $\mathbf{J}^{\mathrm{b}}_{\boldsymbol{\varphi}}$ are zero because

$$\int_0^{T_{\mathrm{o}}} \mathbf{s}_2^{\mathrm{H}}(t-\tau^{\mathrm{b}})\dot{\mathbf{s}}_2(t-\tau^{\mathrm{b}})\mathrm{d}t = 0, \tag{44}$$

$$\int_0^{T_{\mathrm{o}}} \mathbf{s}_2(t-\tau^{\mathrm{b}})\mathbf{s}_2^{\mathrm{H}}(t-\tau^{\mathrm{b}})\mathrm{d}t = N_{\mathrm{s}}\mathbf{I}_{N_{\mathrm{B}}}. \tag{45}$$

In forward transmission, the subscripts "1" and "2" should be interchanged in (43) and the superscript "b" replaced by "f". For example, from $J^{\mathrm{b}}_{\theta_1\phi_1}$ in (43g), we can calculate $J^{\mathrm{f}}_{\theta_2\phi_2} = \gamma\beta^{\mathrm{f}^2}(\mathbf{a}_1^{\mathrm{T}}\mathbf{F}_1\mathbf{F}_1^{\mathrm{H}}\mathbf{a}_1^*)(\mathbf{p}_2^{\mathrm{H}}\mathbf{P}_{\mathbf{W}_2}\mathbf{k}_2)$, which goes in row 3, column 4 in the forward-transmission counterpart of (20).

APPENDIX B
PROOF OF THEOREM 1

Define the vector of all unknown parameters as $\mathbf{v} = [\mathbf{x}^{\mathrm{T}}, \mathbf{z}_1^{\mathrm{T}}, \mathbf{z}_2^{\mathrm{T}}]^{\mathrm{T}}$, then the FIM of $\mathbf{v}$ based on the first and second observations are, respectively,

$$\mathbf{J}_{\mathbf{v}}^{(1)} = \begin{bmatrix} \mathbf{J}_{\mathbf{x}}^{(1)} & \mathbf{J}_{\mathbf{x},\mathbf{z}_1}^{(1)} & \mathbf{0} \\ \mathbf{J}_{\mathbf{x},\mathbf{z}_1}^{\mathrm{T}(1)} & \mathbf{J}_{\mathbf{z}_1}^{(1)} & \mathbf{0} \\ \mathbf{0} & \mathbf{0} & \mathbf{0} \end{bmatrix}, \ \mathbf{J}_{\mathbf{v}}^{(2)} = \begin{bmatrix} \mathbf{J}_{\mathbf{x}}^{(2)} & \mathbf{0} & \mathbf{J}_{\mathbf{x},\mathbf{z}_2}^{(2)} \\ \mathbf{0} & \mathbf{0} & \mathbf{0} \\ \mathbf{J}_{\mathbf{x},\mathbf{z}_2}^{\mathrm{T}(2)} & \mathbf{0} & \mathbf{J}_{\mathbf{z}_2}^{(2)} \end{bmatrix}$$

Since the two observations are independent,

$$\mathbf{J}_{\mathbf{v}} = \begin{bmatrix} \mathbf{J}_{\mathbf{x}}^{(1)} + \mathbf{J}_{\mathbf{x}}^{(2)} & \mathbf{J}_{\mathbf{x},\mathbf{z}_1}^{(1)} & \mathbf{J}_{\mathbf{x},\mathbf{z}_2}^{(2)} \\ \mathbf{J}_{\mathbf{x},\mathbf{z}_1}^{\mathrm{T}(1)} & \mathbf{J}_{\mathbf{z}_1}^{(1)} & \mathbf{0} \\ \mathbf{J}_{\mathbf{x},\mathbf{z}_2}^{\mathrm{T}(2)} & \mathbf{0} & \mathbf{J}_{\mathbf{z}_2}^{(2)} \end{bmatrix} \tag{46}$$

Consequently, EFIM of $\mathbf{x}$ is given by Schur complement as

$$\begin{aligned}\mathbf{J}_{\mathbf{x}}^{\mathrm{e}} &= \mathbf{J}_{\mathbf{x}}^{(1)} + \mathbf{J}_{\mathbf{x}}^{(2)} \\ &\quad - \mathbf{J}_{\mathbf{x},\mathbf{z}_1}^{(1)}\left(\mathbf{J}_{\mathbf{z}_1}^{(1)}\right)^{-1}\mathbf{J}_{\mathbf{x},\mathbf{z}_1}^{\mathrm{T}(1)} - \mathbf{J}_{\mathbf{x},\mathbf{z}_2}^{(2)}\left(\mathbf{J}_{\mathbf{z}_2}^{(2)}\right)^{-1}\mathbf{J}_{\mathbf{x},\mathbf{z}_2}^{\mathrm{T}(2)}\end{aligned} \tag{47}$$

Note that the first and third term in (47) represent the Schur complement of $\mathbf{x}$ with respect to $\mathbf{z}_1$ obtained from the first process, while the second and fourth term represent the Schur complement of $\mathbf{x}$ with respect to $\mathbf{z}_2$ obtained from the second process. In other words,

$$\mathbf{J}_{\mathbf{x}}^{\mathrm{e}} = \mathbf{J}_{\mathbf{x}}^{\mathrm{e},1} + \mathbf{J}_{\mathbf{x}}^{\mathrm{e},2}. \tag{48}$$

ACKNOWLEDGMENT

The authors would like to thank Dr. Xiangyun Zhou of the Research School of Engineering at the Australian National University for his valuable feedback on this work.

REFERENCES

[1] R. D. Taranto, S. Muppirisetty, R. Raulefs, D. Slock, T. Svensson, and H. Wymeersch, "Location-aware communications for 5G networks: How location information can improve scalability, latency, and robustness of 5G," *IEEE Signal Process. Mag*, vol. 31, no. 6, pp. 102–112, Nov. 2014.

[2] I. F. Akyildiz, S. Nie, S.-C. Lin, and M. Chandrasekaran, "5G roadmap: 10 key enabling technologies," *Comput. Netw.*, vol. 106, pp. 17–48, 2016.

[3] J. C. Aviles and A. Kouki, "Position-aided mm-wave beam training under NLOS conditions," *IEEE Access*, vol. 4, pp. 8703–8714, 2016.

[4] N. Akbar, S. Yan, N. Yang, and J. Yuan, "Mitigating pilot contamination through location-aware pilot assignment in massive MIMO networks," in *Proc. IEEE Globecom Workshops*, Dec. 2016, pp. 1–6.

[5] L. S. Muppirisetty, T. Svensson, and H. Wymeersch, "Spatial wireless channel prediction under location uncertainty," *IEEE Trans. Wireless Commun.*, vol. 15, no. 2, pp. 1031–1044, Feb. 2016.

[6] B. Ma, B. Niu, Z. Wang, and V. W. S. Wong, "Joint power and channel allocation for multimedia content delivery using millimeter wave in smart home networks," in *Proc. IEEE Global Commun. Conf.*, Dec. 2014, pp. 4745–4750.

[7] N. Garcia, H. Wymeersch, E. G. Ström, and D. Slock, "Location-aided mm-wave channel estimation for vehicular communication," in *Proc. IEEE 17th Int. Workshop Signal Process. Adv. Wireless Commun.*, Jul. 2016, pp. 1–5.

[8] K. Witrisal *et al.*, "High-accuracy localization for assisted living: 5G systems will turn multipath channels from foe to friend," *IEEE Signal Process. Mag*, vol. 33, no. 2, pp. 59–70, Mar. 2016.

[9] "5G-PPP". 5G Automotive Vision: White Paper on Automotive Vertical Sector. Accessed: Dec. 6, 2018. [Online]. Available: https://5g-ppp.eu/wp-content/uploads/2014/02/5G-PPP-White-Paper-on-Automotive-Vertical-Sectors.pdf

[10] "Ericsson". 5G Use Cases. Accessed: Dec. 6, 2018. [Online]. Available: https://www.ericsson.com/en/5g/use-cases

[11] J. Qiu, D. Grace, G. Ding, M. D. Zakaria, and Q. Wu, "Air-ground heterogeneous networks for 5G and beyond via integrating high and low altitude platforms," *IEEE Wireless Commun.*, vol. 26, no. 6, pp. 140–148, Dec. 2019.

[12] J. G. Andrews *et al.*, "What will 5G be?" *IEEE J. Sel. Areas Commun.*, vol. 32, no. 6, pp. 1065–1082, Jun. 2014.
[13] Z. Pi and F. Khan, "An introduction to millimeter-wave mobile broadband systems," *IEEE Commun. Mag*, vol. 49, no. 6, pp. 101–107, Jun. 2011.
[14] T. S. Rappaport *et al.*, "Millimeter wave mobile commun. for 5G cellular: It will work!" *IEEE Access*, vol. 1, pp. 335–349, 2013.
[15] R. W. Heath, N. G.-Prelcic, S. Rangan, W. Roh, and A. M. Sayeed, "An overview of signal processing techniques for millimeter wave MIMO systems," *IEEE J. Sel. Topics Signal Process.*, vol. 10, no. 3, pp. 436–453, Apr. 2016.
[16] O. Orhan, E. Erkip, and S. Rangan, "Low power analog-to-digital conversion in millimeter wave systems: Impact of resolution and bandwidth on performance," in *Proc. IEEE Inf. Theory App. Workshop*, Feb. 2015, pp. 191–198.
[17] M. D. Larsen, A. L. Swindlehurst, and T. Svantesson, "Performance bounds for MIMO-OFDM channel estimation," *IEEE Trans. Signal Process.*, vol. 57, no. 5, pp. 1901–1916, May 2009.
[18] Y. Shen and M. Z. Win, "Performance of localization and orientation using wideband antenna arrays," in *Proc. IEEE Int. Conf. Ultra-Wideband*, Sep. 2007, pp. 288–293.
[19] Y. Shen and M. Z. Win, "On the accuracy of localization systems using wideband antenna arrays," *IEEE Trans. Commun.*, vol. 58, no. 1, pp. 270–280, Jan. 2010.
[20] Y. Shen and M. Z. Win, "Fundamental limits of wideband localization – Part I: A general framework," *IEEE Trans. Inf. Theory*, vol. 56, no. 10, pp. 4956–4980, Oct. 2010.
[21] Y. Shen, H. Wymeersch, and M. Z. Win, "Fundamental limits of wideband localization – Part II: Cooperative networks," *IEEE Trans. Inf. Theory*, vol. 56, no. 10, pp. 4981–5000, Oct. 2010.
[22] C. Huang, L. Liu, C. Yuen, and S. Sun, "Iterative channel estimation using LSE and sparse message passing for MmWave MIMO systems," *IEEE Trans. Signal Process.*, vol. 67, no. 1, pp. 245–259, Jan. 2019.
[23] X. Gao, L. Dai, S. Zhou, A. M. Sayeed, and L. Hanzo, "Wideband beamspace channel estimation for millimeter-wave MIMO systems relying on lens antenna arrays," *IEEE Trans. Signal Process.*, vol. 67, no. 18, pp. 4809–4824, Sep. 2019.
[24] D. Fan, F. Gao, G. Wang, Z. Zhong, and A. Nallanathan, "Angle domain signal processing-aided channel estimation for indoor 60-GHz TDD/FDD massive MIMO systems," *IEEE J. Sel. Areas Commun.*, vol. 35, no. 9, pp. 1948–1961, 2017.
[25] A. Shahmansoori, G. E. Garcia, G. Destino, G. S.-Granados, and H. Wymeersch, "Position and orientation estimation through millimeter-wave mimo in 5G systems," *IEEE Trans. Wireless Commun.*, vol. 17, no. 3, pp. 1822–1835, Mar. 2018.
[26] A. Guerra, F. Guidi, and D. Dardari, "Single-anchor localization and orientation performance limits using massive arrays: MIMO vs. beamforming," *IEEE Trans. Wireless Commun.*, vol. 17, no. 8, pp. 5241–5255, Aug. 2018.
[27] Z. Abu-Shaban, X. Zhou, T. Abhayapala, G. S.-Granados, and H. Wymeersch, "Error bounds for uplink and downlink 3D localization in 5G millimeter wave systems," *IEEE Trans. Wireless Commun.*, vol. 17, no. 8, pp. 4939–4954, Aug. 2018.
[28] Z. Sahinoglu, S. Gezici, and I. Guvenc, *Ultra-Wideband Positioning Systems : Theoretical Limits, Ranging Algorithms, and Protocols*. Cambridge, U.K.: Cambridge Univ. Press, 2008.
[29] M. Pelka, D. Amann, M. Cimdins, and H. Hellbriick, "Evaluation of time-based ranging methods: Does the choice matter?" in *Proc. 14th Workshop Positioning, Navigation Commun.*, Oct. 2017, pp. 1–6.
[30] J.-Y. Lee and R. A. Scholtz, "Ranging in a dense multipath environment using an UWB radio link," *IEEE J. Sel. Areas Commun.*, vol. 20, no. 9, pp. 1677–1683, Dec. 2002.
[31] N. A. H. Duisterwinkel, E. H. A. Puts, and H. J. Wörtche, "Asymmetric multi-way ranging for resource-limited nodes," in *Ad Hoc Networks*, Y. Zhou and T. Kunz, Eds. Berlin, Germany: Springer, 2017, pp. 50–63.
[32] V. Sark, E. Grass, and J. Gutiérrez, "Multi-way ranging with clock offset compensation," in *Proc. Adv. Wireless Opt. Commun.*, Nov. 2015, pp. 68–71.
[33] Z. A.-Shaban, H. Wymeersch, T. Abhayapala, and G. S.-Granados, "Distributed two-way localization bounds for 5G mmwave systems," in *Proc. IEEE Globecom Workshops*, Dec. 2018, pp. 1–6.
[34] E. Leitinger, P. Meissner, C. Rüdisser, G. Dumphart, and K. Witrisal, "Evaluation of position-related information in multipath components for indoor positioning," *IEEE J. Sel. Areas Commun.*, vol. 33, no. 11, pp. 2313–2328, Nov. 2015.
[35] R. Mendrzik, H. Wymeersch, G. Bauch, and Z. A.-Shaban, "Harnessing NLOS components for position and orientation estimation in 5G millimeter wave MIMO," *IEEE Trans. Wireless Commun.*, vol. 18, no. 1, pp. 93–107, Jan. 2019.
[36] C. E. O'Lone, H. S. Dhillon, and R. M. Buehrer, "Single-anchor localizability in 5G millimeter wave networks," *IEEE Wireless Commun. Lett.*, vol. 9, no. 1, pp. 65–69, Jan. 2020.
[37] S. M. Kay, *Fundamentals of Statistical Signal Processing: Estimation Theory*. Englewood Cliffs, NJ, USA: Prentice-Hall, Inc., 1993.
[38] A. Goldsmith, *Wireless Communications*. Cambridge, U.K.: Cambridge Univ. Press, 2005.
[39] M. Yajima and T. Hasegawa, "Beam pointing error of wideband planar phased array antennas with reduced true-time-delay devices," in *Proc. IEEE Int. Conf. Commun.*, Jun. 2006, vol. 9, pp. 4161–4166.
[40] Z. A.-Shaban, H. Wymeersch, X. Zhou, G. S.-Granados, and T. Abhayapala, "Random-phase beamforming for initial access in millimeter-wave cellular networks," in *Proc. IEEE GLOBECOM Conf.*, Dec. 2016, pp. 1–6.

Zohair Abu-Shaban (Senior Member, IEEE) received the M.Sc. degree in electrical and electronic engineering from the Imperial College London in 2010 and the Ph.D. degree in electrical and electronic engineering from the Australian National University in 2018. During his Ph.D. degree, he was a Visiting Research Scholar with the Universitat Autónoma de Barcelona, Spain, and Chalmers University of Technology, Sweden. Prior to starting his Ph.D. degree, he was an Early-Stage Researcher with the University of Luxembourg, from 2012 to 2014, pursuing research in collaboration with SES S.A, funded by the National Research Fund, Luxembourg. He is currently a Postdoctoral Research Fellow with the University of New South Wales, Australia. During his career, he received several recognitions, including the Department Prize for Outstanding Achievement from the Imperial College London and the Best Ph.D. Thesis Award from the Australian Communication Theory Workshop, 2019 and the European Commission's Marie Curie Fellowship to conduct research on 5G localization and tracking in 2020–2022 at Chalmers University of Technology, Sweden.

Henk Wymeersch (Senior Member, IEEE) received the Ph.D. degree in electrical engineering/applied sciences from Ghent University, Belgium, in 2005. He is currently a Professor of communication systems with the Department of Electrical Engineering, Chalmers University of Technology, Sweden. He is also a Distinguished Research Associate with the Eindhoven University of Technology. Prior to joining Chalmers, he was a Postdoctoral Researcher with the Laboratory for Information and Decision Systems at the Massachusetts Institute of Technology from 2005 to 2009. His current research interests include the convergence of communication and sensing, in a 5G and Beyond 5G context. Prof. Wymeersch served as an Associate Editor for IEEE COMMUNICATION LETTERS (2009–2013), IEEE TRANSACTIONS ON WIRELESS COMMUNICATIONS (since 2013), and IEEE TRANSACTIONS ON COMMUNICATIONS (2016–2018). For 2019–2021, he is a IEEE Distinguished Lecturer with the Vehicular Technology Society.

Thushara D. Abhayapala (Senior Member, IEEE) received the B.E. (Hons.) degree in engineering and the Ph.D. degree in telecommunications engineering from Australian National University (ANU), Canberra, ACT, Australia, in 1994 and 1999, respectively. He held a number of leadership positions including Deputy Dean of the College of Engineering and Computer Science (2015–2019), Head of the Research School of Engineering, ANU (2010–2014), and the Leader of the Wireless Signal Processing Program, National ICT Australia (NICTA) from 2005–2007. He worked with the industry for two years, before his doctoral study and has active collaboration with a number of companies. Among many contributions, he is one of the first researchers to use spherical harmonic based eigen-decomposition in microphone arrays and to propose the concept of spherical microphone arrays; novel contributions on the multizone sound field reproduction problem; was one of the first to show the fundamental limits of spatial sound field reproduction using arrays of loudspeakers and spherical harmonics. He has supervised 39 Ph.D. students and coauthored more than 290 peer-reviewed papers. His research interests are in the areas of spatial audio and acoustic signal processing, and multichannel signal processing. He was an Associate Editor for IEEE/ACM TRANSACTION ON AUDIO, SPEECH, AND LANGUAGE PROCESSING and was a member of the Audio and Acoustic Signal Processing Technical Committee (2011–2016) of the IEEE Signal Processing Society. He is a fellow of Engineers Australia (IEAust).

Gonzalo Seco-Granados (Senior Member, IEEE) received the Ph.D. degree in telecommunications engineering from the Universitat Politecnica de Catalunya, Spain, in 2000, and the MBA degree from the IESE Business School, Spain, in 2002. From 2002 to 2005, he was a member of the European Space Agency, where he was involved in the design of the Galileo System. In 2015 and 2019, he was a Fulbright Visiting Researcher at the University of California, Irvine, USA. He is currently Professor with the Department of Telecommunication, Universitat Autònoma de Barcelona, where he has served as Vice Dean of the Engineering School during 2011-2019. His research interests include satellite and terrestrial localization systems. Since 2018, he has been serving as a member of the Sensor Array and Multichannel Technical Committee for the IEEE Signal Processing Society. Since 2019, he is President of the Spanish Chapter of the IEEE Aerospace and Electronic Systems Society.